THESIS FOR THE DEGREE OF DOCTOR OF PHILOSOPHY

Weld Cracking of Precipitation Hardening Ni-based Superalloys

Investigation of repair welding characteristics and susceptibility towards strain age cracking

Fabian Hanning

Department of Industrial and Materials Science
CHALMERS UNIVERSITY OF TECHNOLOGY
Gothenburg, Sweden

Weld Cracking of Precipitation Hardening Ni-based Superalloys

Investigation of repair welding characteristics and susceptibility towards strain age cracking

Fabian Hanning

ISBN 978-91-7905-258-4

Doktorsavhandlingar vid Chalmers tekniska högskola
Ny serie nr 4725
ISSN 0346-718X

Department of Industrial and Materials Science
Chalmers University of Technology
SE-412 96 Gothenburg
Sweden
Telephone + 46 (0)31-772 1000

Printed by Chalmers digitaltryck
Gothenburg, Sweden 2020

Weld Cracking of Precipitation Hardening Ni-based Superalloys

Investigation of repair welding characteristics and susceptibility towards strain age cracking

Fabian Hanning

Department of Industrial and Materials Science
Chalmers University of Technology

Abstract

High temperature resistance and strength requirements make nickel-based superalloys the material of choice for the hot section of aero engines. Fabrication in terms of combining wrought and cast parts in the manufacturing of hot structural components enables component optimisation via the use of wrought high-strength parts, where geometrical constraints allow, and cast parts to produce complex geometries. Such an approach requires that the materials involved are weldable. Due to the complex microstructure of precipitation hardening nickel-based superalloys, welding comes with the risk of weld cracking, more specifically solidification cracking, heat affected zone (HAZ) liquation cracking and strain age cracking (SAC). While the first two types require a liquid phase to be present, SAC occurs during heating to post-weld heat treatment, in which age-hardening reactions coincide with the relaxation of weld residual stresses. Increasing engine operating temperatures as well as the intermittent cycling of land-based gas and steam turbines motivates research on the weldability of highly temperature-stable alloys.

Hence, the main objective of this work has been the investigation and analysis of microstructural changes and their effect on weldability in terms of susceptibility towards weld cracking of the nickel-based superalloys Haynes® 282® and ATI 718Plus®. This has been addressed by the means of repair-welding studies and a simulative test approach using a Gleeble system. Microstructural changes were found to significantly affect HAZ cracking in cast ATI 718Plus®, where high amounts of Laves phase showed an increased resistance towards cracking. Haynes® 282® shows good weld-cracking resistance, as no HAZ cracks were present after multi-pass weld operations and subsequent post weld heat treatments. A simulative Gleeble test was developed to provide more data on ductility in the SAC temperature range and its dependence on ongoing microstructural changes during thermal exposure. Comparison with Waspaloy showed that the high resistance of Haynes® 282® towards SAC is correlated with the moderate age-hardening kinetics of the alloy and the rapid formation of a grain boundary strengthening carbide network. Furthermore, grain size was found to be a major factor affecting ductility and hence SAC susceptibility.

Keywords: Nickel-based superalloys, welding, weldability, post-weld heat treatment, weld cracking, hot cracking, strain age cracking, Haynes 282, ATI 718Plus, Waspaloy, Gleeble

Preface

This doctoral thesis is based on work performed at the Department of Industrial and Materials Science between October 2015 and March 2020. The project has been carried out under the supervision of Assoc. Professor Joel Andersson.

The thesis consists of an introductory part followed by the appended papers:

Paper I A Review of Strain Age Cracking in Nickel-based Superalloys
Fabian Hanning and Joel Andersson
Proceedings of the 7th International Swedish Production Symposium, 2016

Paper II Weldability of wrought Haynes® 282® repair welded using manual gas tungsten arc welding
Fabian Hanning and Joel Andersson
Welding in the World, 62:39-45, 2018

Paper III Advanced microstructural characterization of cast ATI 718Plus® - effect of homogenization heat treatments on secondary phases and repair welding behaviour
Fabian Hanning, Abdul Khaliq Khan, Joel Andersson, Olanrewaju Ojo
Welding in the world – article online at https://doi.org/10.1007/s40194-020-00851-0

Paper IV Investigation of the effect of short exposure in the temperature range of 750–950 °C on the ductility of Haynes® 282® by advanced microstructural characterization
Fabian Hanning, Abdul Khaliq Khan, Joachim Steffenburg-Nordenström, Olanrewaju Ojo, Joel Andersson
Metals 2019, Volume 9, Issue 12, 1357

Paper V Effect of short-term isothermal exposure on the ductility signature of Waspaloy in the temperature range of 750–950 °C – a comparison with Haynes® 282®
Fabian Hanning, Abdul Khaliq Khan, Olanrewaju Ojo, Joel Andersson
Submitted for journal publication

Paper VI The effect of grain size on the susceptibility towards strain age cracking of wrought Haynes® 282®
Fabian Hanning, Gurdit Singh, Joel Andersson
Swedish Production Symposium 2020 – accepted for presentation

Contribution to the appended papers

Paper I: Fabian Hanning conducted the literature review and wrote the paper. Joel Andersson contributed discussion, paper writing, and corrections.

Paper II: Joel Andersson planned the study. Fabian Hanning planned and executed the microstructural investigations, analysed the results and wrote the paper with discussion input and corrections from Joel Andersson.

Paper III: Joel Andersson planned the repair trials. Fabian Hanning planned and executed the microstructural investigations and analysis. Abdul Khaliq Khan performed the TEM work and provided input for the analysis of the results. Fabian Hanning wrote the paper. Joel Andersson and Olanrewaju Ojo contributed discussion and paper editing.

Paper IV: Fabian Hanning planned the study and carried out experimental work involving Gleeble testing and microstructural analysis. FE simulations were carried out by Joachim Steffenburg-Nordenström. Abdul Khaliq Khan performed TEM work and provided input for the analysis of the results and paper editing. Fabian Hanning wrote the paper. Joel Andersson and Olanrewaju Ojo contributed discussion and paper editing.

Paper V: Fabian Hanning planned the study and carried out experimental work involving Gleeble testing and microstructural analysis. Abdul Khaliq Khan performed TEM work and provided input for the analysis of the results and paper editing. Fabian Hanning wrote the paper. Joel Andersson and Olanrewaju Ojo contributed discussion and paper editing.

Paper VI: Fabian Hanning planned the study and carried out experimental work, including Gleeble testing, and part of the microstructural characterisation. Gurdit Singh carried out part of the microstructural characterisation and analysis of results. Fabian Hanning wrote the paper. Joel Andersson contributed discussion of results and paper editing.

Papers not appended to the thesis

Measurement of the thermal cycle in the base metal heat affected zone of cast ATI®718Plus™ during manual multi-pass TIG welding

Fabian Hanning, Kjell Hurtig, Joel Andersson
Procedia Manufacturing Vol. 25 (2028) pp. 443-449

The Influence of Base Metal Microstructure on Weld Cracking in Manually GTA Repair Welded Cast ATI 718Plus®

Fabian Hanning, Joel Andersson
Proceedings of the 9th International Symposium on Superalloy 718 & Derivatives: Energy, Aerospace, and Industrial Applications, 2018, pp. 917-928

Microstructure modelling of laser metal powder directed energy deposition of alloy 718

Chamara Kumara, Andreas Segerstark, Fabian Hanning, Nikhil Dixit, Shrikant Joshi, Johan Moverare, Per Nylén
Additive Manufacturing, vol 25, pp. 357-364

Predicting the Microstructural Evolution of Electron Beam Melting of Alloy 718 with Phase-Field Modeling

Chamara Kumara, Dunyong Deng, Fabian Hanning, Morten Raanes, Johan Moverare, Per Nylén
Metallurgical and Materials Transactions A, Vol. 50, Issue 5, pp. 2527-2537

Microstructure evolution of the Gleeble-simulated heat-affected zone of Ni-based superalloy

Łukasz Rakoczy, Fabian Hanning, Joel Andersson, Małgorzata Grudzień-Rakoczy, Rafal Cygan, Anna Zielińska-Lipiec
MATEC Web of Conferences 287, 06002 (2019) - 6th International BAPT Conference "Power Transmissions 2019"

Table of Contents

1. Introduction

The hot section of aero engines and of gas turbines in general represents a severe environment for the materials being used there. The high temperature combined with the requirements for high strength and resistance to creep, fatigue, and hot corrosion narrow down the list of applicable materials. Since their development in the mid-20th century, nickel-based superalloys have been the material of choice for this demanding application [1].

Large structural components such as engine housings or turbine exhaust casings have traditionally been manufactured as a single-piece casting. This enables the production of parts with complex geometries but comes with the drawback of reduced strength as compared to wrought material. An optimisation strategy is the so-called assembly approach, in which large structural components are manufactured out of small parts that are joined together by welding [2]. Taking advantage of the high strength of wrought material when allowed by the geometrical constraints enables weight savings while still allowing for the production of complex shaped components. Furthermore, by eliminating the need for large castings, the lead time can be reduced and production costs can be lowered.

This fabrication concept requires the materials involved to be readily weldable; the complex microstructure of nickel-based superalloys, however, often results in challenges. For several years, the standard material has been Alloy 718 due to its temperature stability up to ~650 °C and its adequate fabricability [3]. Because the efficiency of the combustion process increases with temperature, jet engine development has begun to require new materials that are applicable in even more severe environments.

The use of materials with increased thermal stability often goes hand in hand with a higher risk of weld cracking. Hot cracking with crack formation in the fusion zone (solidification cracking) and the heat affected zone (liquation cracking) is often observed in nickel-based superalloys. Different mechanisms exist, and it is not uncommon to find several types of hot cracks after welding. Not all aspects of hot cracking in nickel-based superalloys alloys are well understood, despite the materials having been used for decades. Furthermore, the development of new alloys, such as ATI 718Plus®, requires additional research. Apart from hot cracking phenomena, precipitation hardening superalloys give rise to another major challenge, referred to as strain age cracking (SAC). This cracking phenomenon occurs while heating to solution heat treatment during the post weld heat treatment (PWHT) and is related to the relaxation of weld residual stresses coinciding with the precipitation of hardening phases in the material. Being able to control SAC was one of the main drivers for the development of Alloy 718, for which the sluggish hardening response of its main hardening phase,

gamma double prime, makes it almost immune to SAC. Nevertheless, its limited temperature resistance led to the development of new alloys, one of which is Haynes® 282®. Its maximum service temperature is 150 °C greater than that of Alloy 718, but it uses the gamma prime phase as a hardening precipitate whose more rapid precipitation kinetics may adversely affect cracking resistance. As a fairly new alloy, there is limited data and fundamental knowledge on its weldability and on the mechanisms governing weld cracking in it, motivating more detailed investigations.

1.1. Aim

The aim of this research is to obtain fundamental knowledge on the weld cracking behaviour of nickel-based superalloys. Welding plays a vital role in the production of hot structural components of aero engines, including the possibility of carrying out welding operations for repair and remanufacturing. The first objective of this work is thus to investigate and understand the weld cracking behaviour in a repair welding scenario for the precipitation hardening nickel-based superalloys ATI 718Plus® and Haynes® 282®. The research questions (RQ) formulated out of this objective are

RQ 1: Which weld cracking mechanisms are present during repair operations?

RQ 2: How do microstructural changes resulting from heat treatments affect weld cracking behaviour in a repair welding operation?

In contrast to the sluggish hardening effect of Alloy 718, which is based on the precipitation of the gamma double prime phase, gamma prime hardening materials have a potentially higher susceptibility towards SAC. While the general cause of SAC has been established, the underlying mechanisms are still not fully understood. Furthermore, the use of new alloys requires investigations to evaluate their resistance to this type of weld cracking. This defines the second set of objectives of this work:

- Establishing the current state of research on SAC, including the identification of the most important mechanisms;
- Evaluating available testing methods regarding SAC susceptibility and developing a suitable test approach to investigate the underlying mechanism; and
- Investigating the SAC mechanism in Haynes® 282® and understanding the materials' level of resistance towards cracking.

The related research questions are

RQ 3: How do changes in microstructure affect strain age cracking?

RQ 4: What are the key components of the SAC mechanism in Haynes® 282®?

2. Superalloys for aero engine applications

The severe environment present in the hot sections of aircraft engines requires highly stable materials in terms of temperature resistance and strength at high temperatures. At the turbine inlet, the temperature can now surpass 1500 °C [4]. This exceeds the melting point of nickel-based superalloys by over 100 °C, thus requiring active cooling and the application of thermal barrier coatings to the exposed material. This is even more important for structural components since the precipitation-hardening superalloys applied there usually have to be kept below approximately 800 °C [5].

Generally, nickel-based superalloys can be grouped into three categories based on their strengthening mechanism: solid solution strengthening, precipitation hardening, and oxide dispersion strengthening. While solid solution strengthening is used where strength requirements are moderate and high temperature resistance and good corrosion properties are necessary, precipitation hardening grades are the material of choice for structural applications in aero engines.

Numerous superalloys are commercially available; they all contain a complex mixture of alloying elements that influence their mechanical properties through various effects on the microstructure. The elements Co, Cr, Fe, Mo, Ta and W are used for solid solution strengthening as the deviation of their atomic radii and electronic structure is not too large when compared to the nickel atom. The solubility of these elements is hence quite high [6]. Other alloying elements lead to the formation of secondary phases that can be used for precipitation hardening. Typical hardening precipitates and the alloying elements used to form them are the gamma prime phase γ' (Ni_3Al, Ti) and the gamma double prime γ'' (Ni_3Nb). Several elements result in the formation of carbides that are often used to control the grain size in the material (W, Ta, Ti, Mo, Nb, Cr). Some elements, however, promote the formation of brittle topologically closed packed (TCP) phases (Nb, Ti, V, Zr, Ta, Al, Si) [7]. The potential of some alloying elements to form different phases, some of which are needed to obtain the required properties while others are of a detrimental nature, requires fundamental knowledge about the physical metallurgy as well as precise process control.

2.1. The gamma prime phase (γ')

The gamma prime phase γ' is the main hardening phase for precipitation strengthened nickel-based superalloys. It has the nominal chemical composition Ni_3Al and a face centred cubic crystal structure. Al can be substituted by Ti and Ta; γ' is thus often denoted as $Ni_3(Al,Ti)$ [8]. Its face centred structure, combined with a low mismatch in the lattice parameter, makes γ' coherent with the nickel matrix and allows for homogeneous precipitation within the matrix. This leads to fast precipitation kinetics, while particle growth is slow [9]. For small particle diameters and during earlier stages of ageing, the particle shape is spherical, as shown exemplarily in Figure 1 (a) for Haynes® 282® exposed to 950 °C

for 30 min. Based on lattice mismatch and particle size, the shape can change to cubes or to plates, which reduces the surface energy by matching the structure of the matrix, as shown exemplarily in Figure 1 (b) for γ' found in as cast ATI 718Plus®.

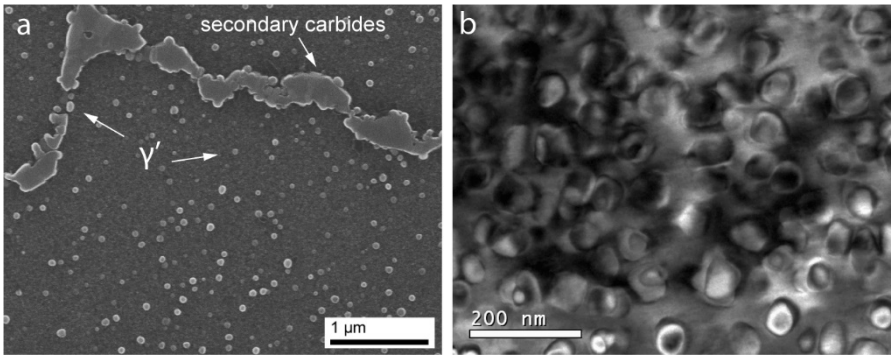

Figure 1: (a) Microstructure of wrought Haynes® 282®, heat treated at 950 °C for 30 min; spherical γ' and secondary carbides at the grain boundaries are indicated by arrows. (b) Cuboidal γ' present in as cast ATI 718Plus®.

2.2. Carbides

Different types of carbides can be present in nickel-based superalloys. Cubic MC-type carbides, rich in Ti, Nb, and Ta, form above the solidus temperature of the matrix and are hence present from the primary manufacturing process. The amount and size can change during the subsequent heat treatments, but some MC carbides normally remain in the material. During heat treatments, secondary carbides can form. These are of the M_6C or $M_{23}C_6$ type and are usually formed by solid state reactions of the type

$$MC + \gamma = M_{23}C_6 + \gamma' \quad (1)$$

Secondary carbides usually form at the grain boundaries and are therefore often intentionally precipitated for grain size control as well as to inhibit grain boundary sliding [10]. If present in long, continuous films, they can, however, have detrimental effects on the mechanical properties and weldability of the alloy.

2.3. Other phases

Beyond the γ' phase being used as a hardening precipitate in most of the precipitation hardening superalloys, weldability issues led to the development of Alloy 718, which instead uses the metastable gamma double prime phase (γ''). This phase is a body centred tetragonal phase with the nominal chemical composition of Ni_3Nb. Like the γ' phase, it is coherent with the nickel matrix, albeit showing significantly larger mismatch. This results in a steeper increase in strength but also in more sluggish precipitation kinetics and reduced thermal stability. As a metastable phase, γ'' decomposes into the

incoherent and stable delta phase (δ), which is accompanied by a loss in strength [10]. The complex chemical composition of superalloys allows for several other phases to be present in the microstructure, notably detrimental TCP phases that can form after long time service exposures [9]. In Nb-bearing alloys such as Alloy 718 and ATI 718Plus®, the hexagonal Laves phase, which affects weldability due to its low melting point, can be present [7]. The presence of Nb segregation in cast materials and welds can cause the formation of the Laves phase, which is not thermodynamically stable at nominal alloy compositions. The presence of a γ'-Laves eutectic significantly extends the solidification range of Nb-bearing alloys and for ATI 718Plus® lies at approximately 1163 °C [11]. Considering that such Laves phase induced melting can be explained by a pseudo-binary system as reported by [11, 12], when exceeding a local Nb concentration of approximately 8 - 9 wt.-%, the formation of a γ-Laves eutectic should be expected during high temperature exposure. Such an increase in Nb concentration can be present from melt segregation or via local enrichment due to the constitutional liquation mechanism. The latter is described in more detail in the following chapter. Borides can have the same effect as carbides if finely dispersed and have been reported to have a positive effect on creep life [13]. Borides can nonetheless have a negative effect on heat affected zone (HAZ) liquation cracking, as further explained below.

3. Processing of nickel-based superalloys

Nickel-based superalloys are generally available in both wrought and cast form. While wrought material exhibits good microstructural homogeneity and high strength, it is not useable for complex shapes without extensive machining, if it is even possible. For cast materials, on the other hand, the shape can be controlled with a much larger degree of freedom. This comes with the disadvantage of a significantly more segregated and inhomogeneous microstructure, resulting in reduced strength. Wrought superalloys are primarily produced using vacuum induction melting (VIM). The obtained ingots are then refined by electro slag re-melting (ESR) and/or vacuum arc re-melting (VAR) techniques [9]. After annealing, drawing and forging, further heat treatments are necessary to obtain the required material properties.

A typical heat treatment procedure is schematically shown in Figure 2. As an initial step, a solution heat treatment is carried out to dissolve secondary phases in the microstructure. Note that such a treatment does not affect primary MC-type carbides since their dissolution temperature lies above the solidus of the matrix. Air cooling or water quenching is used depending on the alloy to prevent microstructural changes during cooling to room temperature. The term ‘mill annealing’ refers to this treatment, representing the material condition typically delivered from the primary manufacturer. Any hardening heat treatments are usually carried out after further manufacturing of components. To achieve the required material properties, age hardening is necessary. In most cases, this is done via a two-step process (cf. Figure 2). The higher aging temperature is used to obtain the desired amount and morphology of secondary carbides, and during the second aging step hardening precipitates, like γ’, are formed in the material. The first step is used to create a supersaturated solid solution during the subsequent aging, which is necessary for the efficient aging of γ’. If a bimodal size distribution is desired, the first step can be further divided into a set of temperatures, as is common practice for Alloy 718 or Waspaloy [14, 15]. The same heat treatment procedure also has to be carried out after welding to relieve weld residual stresses and to obtain uniform properties throughout the component. This can cause problems in the form of weld cracks, as discussed in the following section.

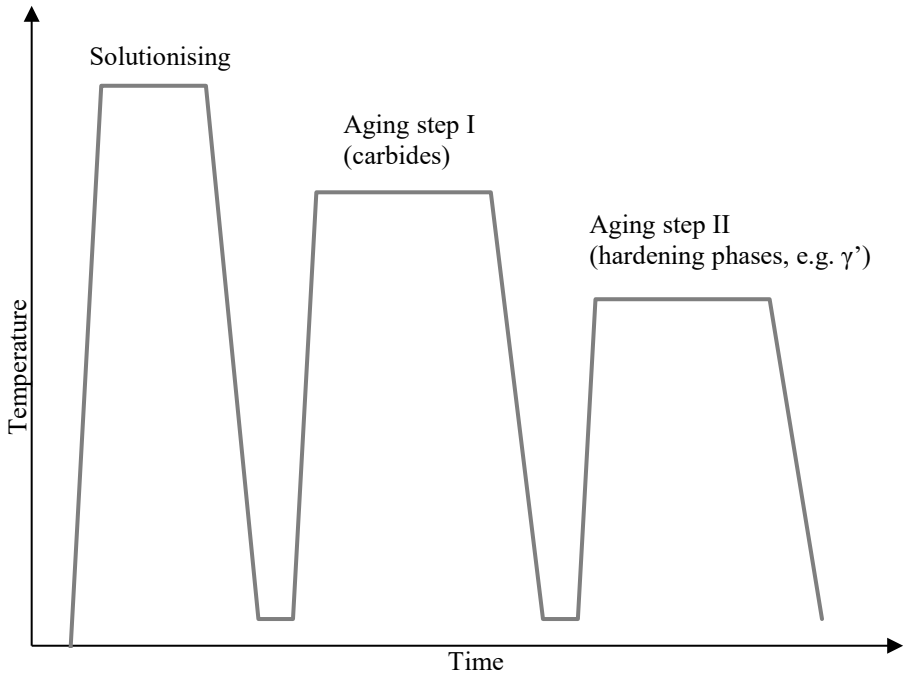

Figure 2: Schematic 2-step heat treatment cycle for nickel-based superalloys.

4. Welding of superalloys

Welding plays a major role in the fabrication of hot structural components using nickel-based superalloys. This is based on the possibility of joining different materials with few limitations on the shape and previous manufacturing steps. One example is the trend of introducing welding to the fabrication of hot structural parts of jet engines. These components, made out of nickel-based superalloys, have traditionally been produced as large single-piece castings [2]. Using welding as a joining technique allows for the combination of high-strength wrought parts and complex shaped cast parts and yields both weight and cost reductions [16]. Welding processes have experienced significant advancements that paved their way into the production of structural components in the aero engine industry. However, the most common techniques used in fabrication are still gas tungsten arc welding (GTAW), laser beam welding (LBW), plasma arc welding (PAW) and electron beam welding (EBW) [17]. Apart from enabling the manufacturing of large structural components, welding is heavily relied on for repair operations. These are often necessary during production but also in maintenance and overhaul operations. The high cost of turbine components often makes repair the more economically feasible alternative when compared to complete replacement of damaged parts.

Especially when joining sophisticated alloys, such as superalloys, high demands are placed on process control and on the weld geometry. The rapid heating and cooling cycle, together with the mechanical restraint from the joint, can create numerous residual stresses in the material [18]. This in turn can lead to cracking and distortion. Furthermore, microstructural changes due to the weld thermal cycle require additional treatments of the welded components. Various PWHT are carried out to relieve weld residual stresses and to obtain the desired microstructural and mechanical properties in the material.

Welding of superalloys can also result in the formation of weld cracks, with the complex microstructure of superalloys generally making these materials difficult to weld. Knowledge of the underlying mechanisms is a requirement for being able to produce crack-free welds, explaining the high research interest in weld cracking phenomena in superalloys [17, 19].

4.1. Weld cracking

The cracking mechanisms occurring in nickel-based superalloys can be divided into different groups, based on the temperature range within which they occur. Cold cracking is usually not directly connected to welding and includes hydrogen embrittlement at ambient temperatures. Warm cracking phenomena, such as strain age cracking and ductility dip cracking, occur at high temperatures in the heat affected zone (and fusion zone during multi pass welding operations) but do not require a liquid phase to be present. They are hence also referred to as solid state cracking. Hot cracking occurs at high

temperatures and requires the presence of liquid phases, with possible crack formation in both the fusion zone (FZ) and heat affected zone (HAZ) [9].

4.1.1.Solidification cracking

Weld solidification cracking occurs in the FZ, where cracks are formed during the passage of the liquid-solid two-phase region upon cooling. Several theories of weld solidification cracking have been proposed during the last 60 years but not all aspects are fully understood yet. In general, two main factors in its occurrence can be identified, namely the presence of restraint and of a susceptible microstructure. The former can result from the formation of thermal stresses during cooling, as a temperature and heating/cooling rate gradient between the fusion zone and base material is present. The restraint is further influenced by the weld bead geometry, workpiece design, and thickness, heat input during welding, and mechanical fixture (external restraint). Early theories include the shrinkage-brittleness theory [20] and the strain theory of hot tearing [21]. These were combined into the generalised theory of super-solidus cracking by Borland in the early 1960s [22]. In general, the solidification process is described as

- Stage 1: Primary dendrite formation in a continuous liquid with relative movement between all phases being possible.
- Stage 2: Dendrite interlocking, leaving only the liquid as a mobile phase.
- Stage 3: Grain boundary development with creation of a semi-continuous network, restricting the liquid phase from moving freely.
- Stage 4: Solidification of the remaining liquid.

It is assumed that cracking occurs exclusively in stage 3, which is referred to as the 'critical solidification range' (CSR), since backfilling would occur at earlier stages. After complete solidification, contraction stresses are compensated uniformly and no cracking occurs.

In general, a short solidification range is beneficial for resistance to cracking, as thermal restraint plays an increasing role at lower temperatures. Due to their high alloying content, nickel-based superalloys are prone to segregation, resulting in the local suppression of the melting point. In particular, minor alloying elements such as P, S, B, C, and Zr have a negative influence on cracking resistance [7, 23] because they are reported to accumulate at grain boundaries and interdendritic areas and form intermetallic compounds, such as M_3B_2 and Ni_7Zr_2 in the case of Inconel 738LC [24, 25]. Alloys containing large amounts of Nb, such as Alloy 718, are especially prone to the formation of cracks due to the strong segregation of this element, which causes the formation of NbC carbides and Laves phase eutectics in interdendritic areas. This is accompanied by a significant reduction in melting point in the

interdendritic areas [16, 26]. The presence of large amounts of eutectic liquid can, however, facilitate backfilling, which reduces the amount of cracks in the material [16, 27, 28].

4.1.2. Heat affected zone liquation cracking

In contrast to weld solidification cracking, which occurs in the FZ of the weld, HAZ liquation cracking is localised to the partially melted zone usually referred to as the PMZ. This zone lies in the HAZ and is in close proximity to the FZ. Its main characteristic is the presence of a liquid fraction, formed when the effective solidus temperature is exceeded during heating. The presence of stresses during subsequent cooling can then cause crack formation. The liquid can form by different mechanisms, namely segregation induced liquation, constitutional liquation and eutectic melting.

Segregation induced liquation is based on the local suppression of the solidus temperature. Elements like S, P, and B are especially known to segregate within the microstructure and are usually enriched near grain boundaries. The segregation behaviour of these elements and their effect on weldability has been thoroughly studied, particularly for Alloy 718 [29–39]. Apart from boron, which has been found to have a positive influence on creep resistance and stress rupture life [13], the general effect of these elements is detrimental and their concentrations are usually kept at a minimum level.

Constitutional liquation can occur if second phase particles (i.e. precipitates) are present in the matrix. The mechanism was originally introduced for maraging steels by Pepe and Savage [40] and was later adapted to explain HAZ liquation cracking in Alloy 718 by Owczarski et al. [41]. A key factor in the mechanism is fast heating, so that particles can survive despite not being thermodynamically stable above the eutectic temperature (assuming the phase interactions can be described by a eutectic system). Under the further assumption of equilibrium conditions at the phase boundary between matrix and particle, a concentration gradient develops around the particle during its subsequent dissolution. When reaching the eutectic temperature, the reaction zone around the particle liquates. It should be noted that the particle itself does not melt, as e.g. TiC has a melting point far above that of the nickel matrix [7]; only the solute enriched reaction zone contributes to the melt formation. This mechanism has been observed especially for Nb-bearing alloys such as Alloy 718 and ALLVAC 718Plus [16, 41] but has also been reported for other precipitation hardening alloys [27, 42–44]. Figure 3 shows an example of constitutional liquation of NbC carbides in cast ATI 718Plus®.

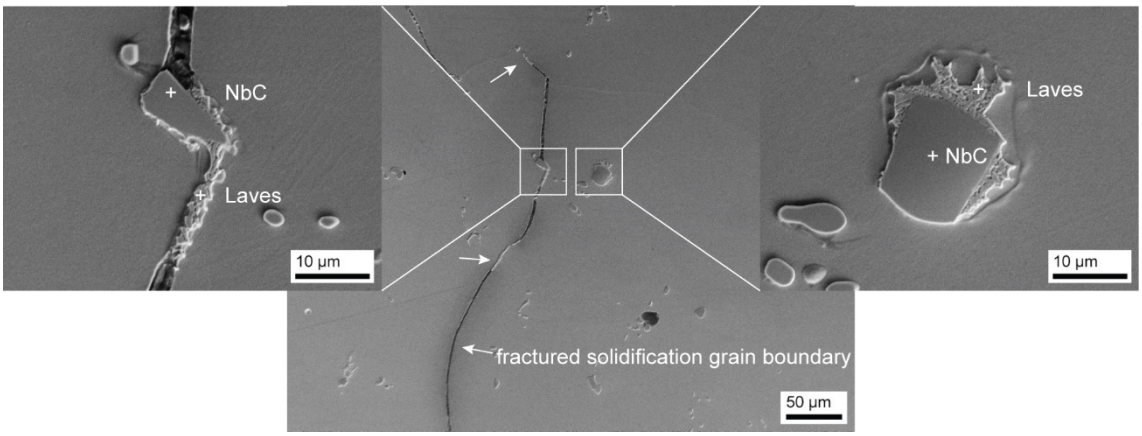

Figure 3: Constitutional liquation in cast ATI 718Plus®, showing the formation of γ-Laves eutectics around NbC particles [45] (PAPER III).

Eutectic melting is only found in cast alloys and relates to the strong segregation in interdendritic areas, as shown in the example of cast ATI 718Plus® in Figure 4. It has been observed in cast Alloy 718 by various authors [16, 19, 46]. Related to their generally more segregated microstructure, cast alloys are considered more susceptible to HAZ liquation cracking than wrought alloys.

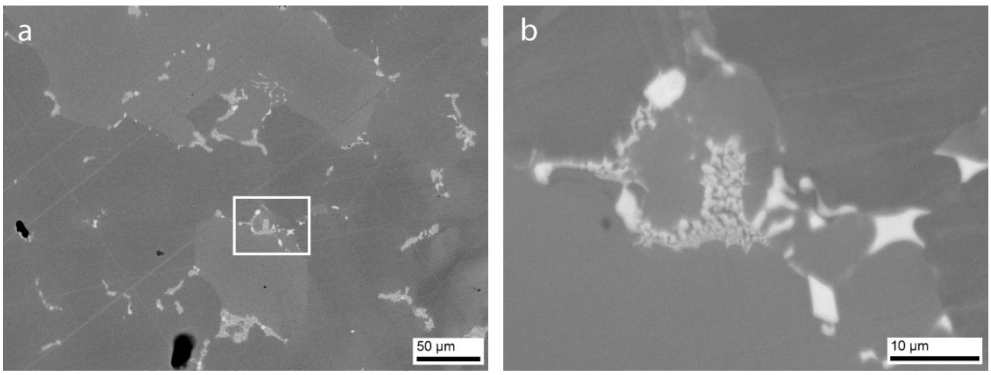

Figure 4: (a) Eutectic melting involving Laves phase in cast ATI 718Plus® in interdendritic areas. (b) Magnified section from (a) showing the structure of the γ-Laves eutectic.

4.1.3. Solid state weld cracking phenomena

In contrast to the hot cracking phenomena described above, solid state cracking, or warm cracking, does not require a liquid phase to be present in the material. Solid state cracks can occur in several alloy systems and material types.

A material group that shows cracks during reheating after welding is the solid solution strengthened nickel-based superalloys. The presence of a dip in ductility over an intermediate temperature range was already found in 1912 by Bengough, who investigated aluminium, copper and copper alloys [47]. Rhines and Wray later reported the presence of a ductility dip below the recrystallisation temperature in copper alloys, nickel alloys, austenitic stainless steels, titanium alloys and aluminium alloys [48].

The mechanism of ductility dip cracking (DDC) proposed by Rhines and Wray is based on grain boundary shearing at temperatures below the recrystallisation temperature [48]. Grain boundary shearing was also found to be the reason for DDC by Arkoosh and Fiore, who investigated Hastelloy X. They attributed localised deformation at the grain boundaries to excessive intragranular carbide precipitation [49]. Later investigations from Ramirez and Lippold [50, 51] and Noecker and DuPont [52, 53] also found an influence of carbides on localised deformation. They however report carbides to be beneficial in inhibiting grain boundary sliding if they precipitate at grain boundaries. Yamaguchi et al. found that sulphur segregation leads to grain boundary embrittlement and hence causes DDC [54]. The negative effects of sulphur and other impurities like phosphorous and hydrogen has also been reported in later studies by Collins et al. [55], Nishimoto et al. [56–58] and Saida et al [59]. However, Ramirez and Lippold found that while impurities have a negative impact, the absence of S and P cannot completely prevent ductility dip cracking [50, 51]. They proposed that the main influencing factor on DDC is grain boundary tortuosity, leading to a more resistant material due to reduced strain concentration. This is in good agreement with the findings of Noecker and DuPont [52, 53] and has also more recently been confirmed by Chen et al [60].

The phenomenon of reheat cracking has been investigated by various authors for austenitic stainless steels and ferritic low alloy CrMoV steels. It has also been referred to as stress relief cracking in some studies, as stress relief has been identified as a main influencing factor. Younger and Baker investigated reheat cracking in austenitic steels and found a relationship between cracking susceptibility and strain-induced intragranular carbide precipitation (TiC, NbC, $M_{23}C_6$) in the temperature range of 550 to 950 °C [61]. Other early studies include that of Bentley, who found that V carbide precipitation in CrMoV steels leads to embrittlement [62]. He concludes that a large amount of finely dispersed carbides leads to the greatest embrittlement (i.e. a low stress relief temperature, favouring nucleation over growth reactions). Fast carbide precipitation in the grain interior during heating has been attributed to a supersaturation of carbide forming elements due to fast cooling after welding [63]. Other researchers found a negative influence of sulphide precipitation [64] and of the presence of carbides at grain boundaries [65]. Dhooge and Vinckier have thoroughly reviewed the literature on reheat cracking in steels and summarise the available mechanisms as follows [66, 67]:

- Intragranular carbide precipitation, leading to relatively weaker grain boundary areas; the precipitation of carbides at grain boundaries has also been reported and is associated with the formation of denuded zones around grain boundaries (i.e. zones with lower alloy content).
- Precipitates at grain boundaries induce void formation or promote boundary decohesion during grain boundary sliding.
- Stress induced segregation of impurities to grain boundaries, leading to embrittlement.

4.1.4.Strain age cracking

The solid state cracking mechanism that can be observed in precipitation hardening nickel-based superalloys is strain age cracking (SAC), also referred to as reheat cracking or PWHT cracking. The general mechanism of SAC was studied in the early 1960s and 70s by various researchers [68–75]. It is generally accepted that the occurrence of cracks during the PWHT cycle is caused by the simultaneous presence of stresses in the HAZ and low ductility in this region. This is explained as follows. During cooling from welding a significant amount of restraint is built up in the HAZ due to thermal stresses and external weld restraint. The former is caused by the temperature gradient present from the base metal to the weld fusion zone. The residual stresses are partially relieved during heating to the PWHT, which coincides with the precipitation of hardening phases (cf. Figure 5) [70].

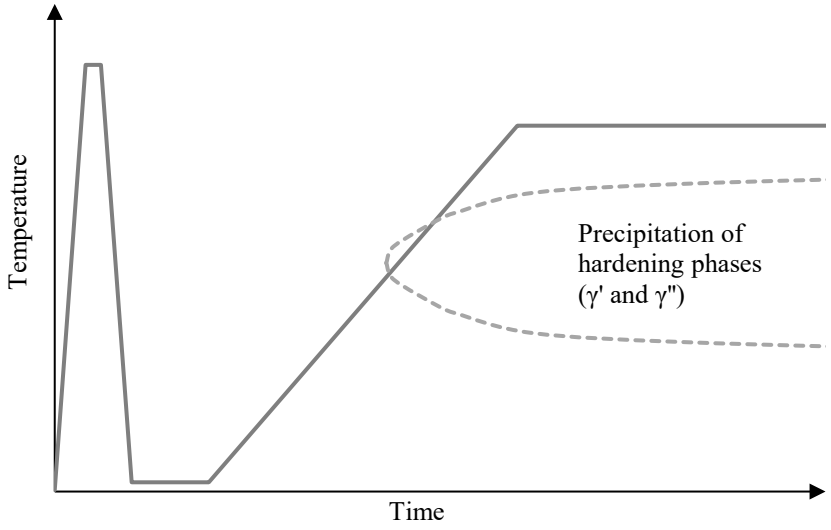

Figure 5: Schematic time-temperature regime for a welding operation followed by heating to PWHT. The dashed line represents the precipitation curve of a TTT diagram [76] (Paper I).

The precipitation reaction is believed to lead to the higher strength of the grain interior as compared to the grain boundaries. The deformation (i.e. stress relaxation) is thus localised to the grain boundaries. When grain boundary sliding is not accompanied by volume deformation, high stresses develop, especially at grain boundary triple points, and intergranular cracks form [48, 61]. Different authors claim an additional effect of contraction stresses due to γ' precipitation based on the difference in lattice parameters of the γ matrix and γ' [69, 70, 77, 78].

4.1.4.1. Chemical composition

SAC is a precipitation-related phenomenon. It is thus strongly influenced by the chemical composition, which has been investigated by various authors [68, 71, 75, 79]. Nonetheless, when examining the effect of trace elements, the results are often contradictory. This is mainly related to the fact that it is difficult, if not impossible, to alter the concentration of one element without changing that of the others at the same time. Combined with the often limited number of different heats available for an investigation, the results have to be interpreted with care. The elements forming the hardening phases have the largest influence on the cracking response. Increased Al+Ti content has been reported to lead to higher cracking susceptibility [70, 73]. This is shown in Figure 6, the so-called Prager-Shira diagram [70]. The figure provided has been updated with more recent alloy compositions; Al+Ti contents above the grey line indicate reduced weldability [76].

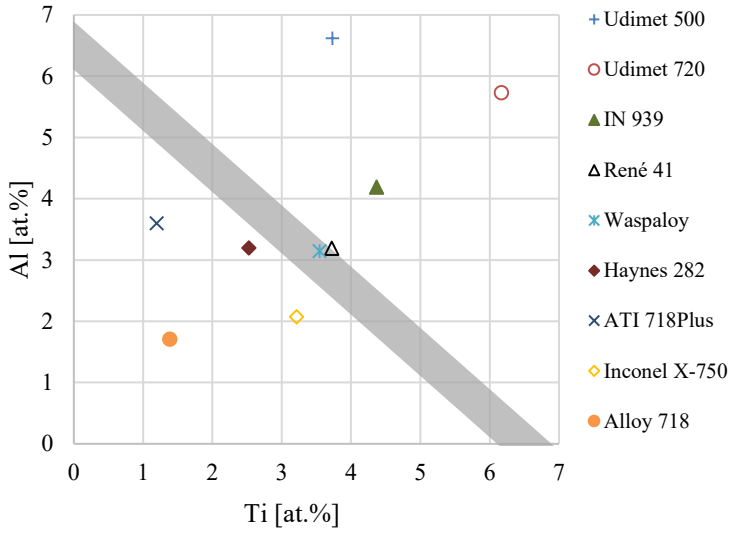

Figure 6: Al and Ti concentrations of some commercially available superalloys; low weldability above grey line [76] (Paper I).

The effect of C has been investigated in several studies. Carbon has been found to be beneficial due to grain size control [72, 75, 80]; however, its effect on HAZ liquation cracking should also be considered when evaluating the overall weldability of an alloy. Other elements like Fe, Mn and S have been reported to not have a significant effect on SAC, while B can have a similar effect to that of C and can increase stress rupture life [13, 75]. Research on the role of B has mostly been related to HAZ liquation cracking in Alloy 718, where it was found to have a negative impact [29–39].

4.1.4.2. Effect of microstructure

Apart from hardening precipitates, the effect of microstructure can be divided into grain size and homogeneity. The former has a positive effect if kept on a low level [79, 81] since the distribution of loads over a larger grain boundary area reduces the local stress level. Inhomogeneities like segregation are more of a concern in cast materials; their effect is generally seen in the form of increased hot cracking susceptibility. If a welded part is already pre-damaged when put through post weld heat treatment, further cracking can be triggered [19].

The hindering of dislocation movement and hence hardening caused by precipitates like γ' is based on the mismatch with the matrix phase, with a higher mismatch leading to an increased hardening effect. An effect of mismatch on the development of contraction stresses and hence on SAC susceptibility has been proposed in early studies [69, 70, 77]. More recent computer simulations by Andersson indicate a positive correlation between negative lattice mismatch and cracking resistance [78]. The lattice parameter change of the γ phase as a function of δ , γ' and γ" has been investigated for Alloy 718 by Liu et al. [82]. They reported a decrease for higher precipitate contents. However, no information is available about the misfit created by the precipitation reactions. Tiley et al. investigated René 88DT by means of synchrotron X-ray and neutron diffraction and reported that the lattice mismatch increased with aging time while initially decreasing as a function of temperature [83]. Another study by Whitmore et al. on Allvac 718Plus showed a small negative lattice mismatch between γ and γ' after aging, following a HAZ simulation with deformation. [84]. Note that the investigation was more focused on morphology and chemical composition. The measurement was conducted at room temperature and consequently does not necessarily reflect the conditions in the PWHT temperature range in terms of lattice parameter misfit. Measurements of the lattice mismatch during creep in a single crystal nickel-based superalloy by Dirand et al. led to the conclusion that the misfit is strongly dependent on temperature, stress and previous plastic deformation [85]. Available data indicate a relationship between lattice parameter misfit and SAC, though quantifiable data collected in the time-temperature range where SAC occurs has yet to be obtained.

4.1.4.3. Effect of material condition and welding process

Crack formation during PWHT is related to low ductility in the HAZ, combined with stress relaxation processes. The localisation to the HAZ is related to its lower strength as compared to the base material. It is thus reasonable that softer base material should decrease susceptibility to SAC. This has been confirmed by several investigations [70, 74, 81, 86, 87]. Fully age hardened base material led to the most severe cracking in the heat affected zone. Over-aged material, on the other hand, has been found to have a beneficial influence on SAC resistance as the lower strength of such a microstructure results in stress relaxation in the base material [81]. The thermal stresses generated during the welding

operation strongly depend on the heat input. This becomes clear when comparing the effects of GTAW and EB welding on SAC. Since low heat input can in turn lead to HAZ liquation cracking [88–90], a balance has to be found to achieve the overall best cracking resistance.

The mechanisms and the main influencing factors related to SAC can be summarised as follows [76]:

- Strain
  - Weld restraint
  - Precipitation-induced stress
- Stress relaxation
  - Initial magnitude of stress
  - Time-temperature regime
  - Young's modulus
- Precipitation kinetics
  - Chemical composition
  - Strain (higher dislocation density facilitates nucleation)
- Stress localisation at grain boundaries
  - Grain size
  - Grain boundary conditions (e.g. precipitates)

4.2. Weld cracking tests

Weldability testing is characterised by the numerous tests that are tailored towards investigating specific cracking phenomena that occur during welding [91, 92]. This can cause poor correlation between studies due to their different setups and test parameters even when the same phenomenon is being investigated. Weld cracking tests can be categorised by the phenomenon they are used to study or by their approach [7]. Using the latter classification, the tests can be divided into representative and simulative tests.

A material's weldability under specified conditions can be evaluated via welding trials. Such tests can provide a realistic benchmark of welding performance and when coupled with microstructural analysis, can provide valuable insight into which weld cracking mechanisms are present under the studied conditions. As such, welding trials are useful as starting points for a larger investigation or to test hypotheses based on simulative test data. Using systematic analysis, some quantitative data such as crack length can be obtained from such tests. Welding trials, however, only cover a limited range of process parameters, and often the boundary conditions during welding, such as restraint level and temperature profile, are not precisely known. Nevertheless welding trials are still used today, often in conjunction with repair welding [45, 93–99].

Simulative tests, on the other hand, use the mechanical and thermal conditions present during welding to investigate weld cracking with a more precisely controlled parameter set. While specialised equipment that includes actual welding exist, e.g. the Varestraint test [100], many methods focus on temperature cycling and mechanical loading. Out of the tests used to study hot cracking phenomena, the hot ductility test (HDT) is one of the more frequently used methods. Here, the thermal cycle in the base metal heat affected zone (HAZ) is simulated by rapid heating and cooling, which is followed by pulling test specimens to fracture for the evaluation of ductility [101, 102]. A set of test temperatures is chosen up to a temperature close to the melting point (T_L), at which point the material cannot sustain any load, and a ductility curve is generated for on-heating and on-cooling cycles. This allows for the investigation of the brittle temperature range (BTR). Figure 7 schematically shows a ductility signature measured during the HDT with important points indicated on the graph. The rapid ductility loss in the on-heating curve is related to the onset of liquation in the material [7]. On-cooling tests are performed by first heating a test specimen to a peak temperature (T_{Peak}), typically 50 °C below the nil-strength temperature (NST).

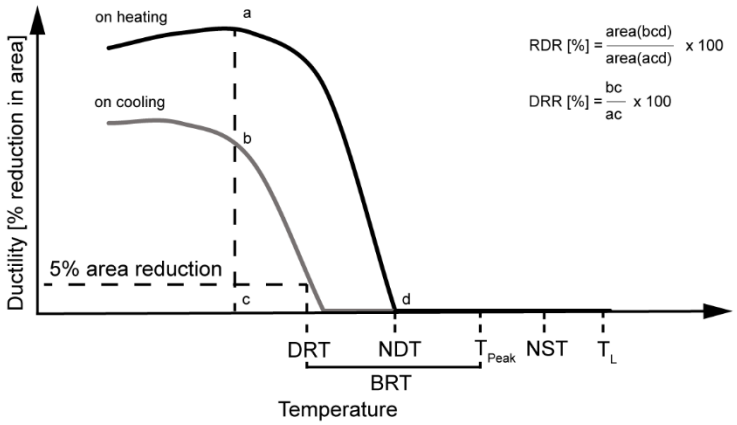

Figure 7: Schematic hot ductility signature curve from the HDT with important temperatures indicated on the graph. Adapted from [16].

Other important parameters that can be obtained from the HDT are the nil-ductility temperature (NDT), ductility recovery temperature (DRT), ductility recovery rate (DRR), and ratio of ductility recovery (RDR). The method makes it possible to study the liquation behaviour in the HAZ during welding and can be used to compare different materials [16].

The HDT is carried out using a Gleeble thermomechanical simulator, which was originally developed at the Rensselaer Polytechnic Institute in the 1950s [103]. The general setup is shown in Figure 8. The machine is capable of heating small test specimens at rates of up to 10^5 °C/s via resistance heating. The machine uses closed-loop temperature control via a thermocouple spot welded to the specimen centre as indicated in Figure 8 (b). Heat is conducted towards the water-cooled jaws, resulting in a

narrow, parabola-shaped temperature distribution in the specimen. If heat conduction into the jaws does not result in the desired cooling rate, the cooling can be accelerated by spraying different quenching mediums onto the specimen. The thermal profile can be simultaneously coupled with mechanical loading, allowing for e.g. the compensation of thermal expansion or pulling samples to fracture while controlling the temperature.

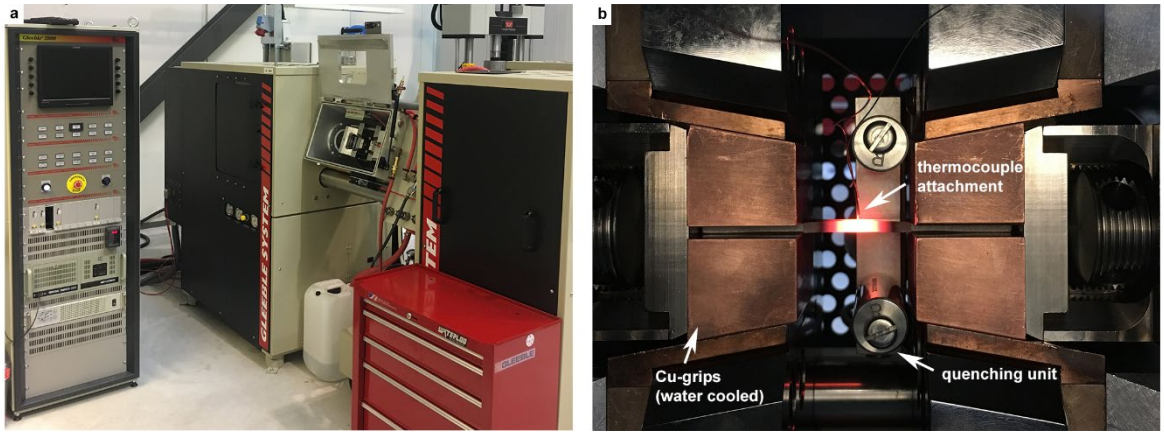

Figure 8: Gleeble 3800 system (a), test specimen during heating, with thermocouple placement, copper grips and quenching unit indicated by white arrows (b).

Several approaches have been followed to investigate SAC, including self-restrained tests such as the circular patch test, constant load rupture (CLR) tests, stress-to-fracture tests, stress relaxation tests and tests measuring ductility [76], as summarised in Table 1.

Table 1: Test methods to investigate SAC in nickel-based superalloys, summarised from [76] (PAPER I).

Type of test	***Advantages/ Disadvantages***
Constant load rupture tests (CLR)	Time to failure measured Does not predict well
Stress relaxation tests	Hard to create material rankings Can provide insight into mechanism
Stress to fracture tests	Does not indicate resistance towards SAC
Tests measuring ductility	Can be used to rank materials Good indicator for SAC susceptibility

One of the more commonly used testing approaches that measures ductility follows the idea of simulating the slow heating to PWHT, combined with acquiring ductility data in the temperature range where SAC occurs. This test is referred to as the constant heating rate test (CHRT) [79]. While for the original test a clamshell furnace was used, the Gleeble thermomechanical simulator enables fast heating and cooling cycles that are comparable to those present during welding. This yields the ability

to add a fast heating and cooling cycle in advance of the CHRT in order to create a microstructure similar to that found in the HAZ of welds where SAC occurs; the thermal cycle of the test is shown schematically in Figure 9. The modified CHRT takes advantage of the more capable testing equipment available today in welding research and enables the screening of different alloys based on their susceptibility towards SAC. The testing of microstructures corresponding to those found in the HAZ of actual welds ensures that the test results can be related to real applications. While requiring a metallographic investigation of tested samples, testing HAZ simulated microstructures also includes the effect of potential weaknesses such as liquation cracks that can form during the welding process. The effect of such a pre-damaged microstructure has been found to negatively affect the performance of the material during simulated PWHT cycles [19].

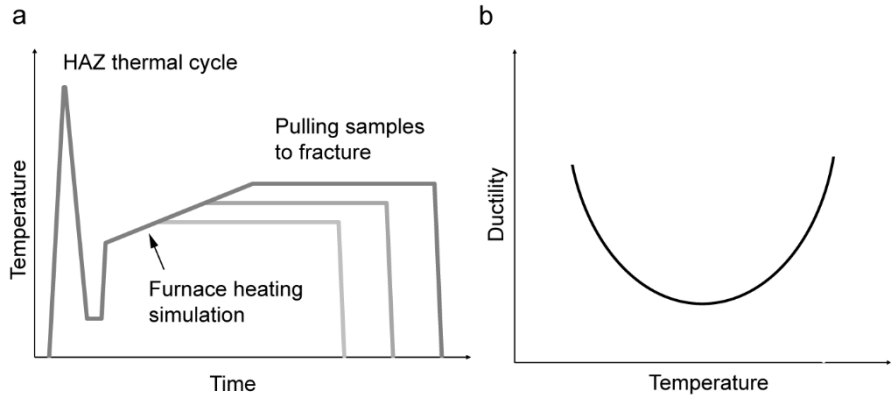

Figure 9: (a) Schematic time-temperature cycle of the modified CHRT test [76] (Paper I). (b) Typical test result showing a drop in ductility.

While useful for screening purposes, such a test does not provide insight into the underlying mechanisms. Since SAC is a precipitation-related cracking phenomenon, investigation of the precipitation kinetics in the SAC temperature range, combined with short exposure times in the range of PWHT heating rates, could provide a better understanding of this cracking phenomenon.

5. Experimental methods

5.1. Materials and heat treatments

Cast ATI 718Plus®

ATI 718Plus® is a derivative of Alloy 718, developed to increase the maximum service temperature. This is achieved by increasing the amount of Al+Ti in the material, which results in the γ' phase being the main hardening precipitate. Its thermal stability is thus increased by ~50 °C as compared to Alloy 718. Initially developed as a wrought material, a cast version was soon available, increasing the applicability of the alloy. Development was carried out in a material affordability initiative in the United States, which resulted in a modified chemical composition of cast ATI 718Plus® with higher Nb content [104, 105]. ATI 718Plus® in the form of investment cast plates has been used in **PAPER III**. The chemical composition is provided in Table 2.

Table 2: Chemical composition in wt.-% of the investment cast ATI 718Plus® studied in this work.

Ni	Cr	Co	Mo	Ti	Al	Fe	Mn	Si	C	B	Nb	W
Bal	20.72	8.34	2.71	0.75	1.50	9.31	0.01	0.04	0.05	0.005	6.02	1.00

Haynes® 282®

Haynes® 282® is a relatively new γ' hardening superalloy [106] that has been developed to provide increased thermal resistance as compared to Alloy 718, which due to its main hardening precipitate the γ'' phase, can withstand temperatures of up to 650 °C. The γ' phase present in Haynes® 282® instead enables a maximum service temperature of 800 °C.

In this thesis, Haynes® 282® has been investigated in the form of a wrought bar (**Paper II**) and a 3.15 mm (1/8 in) rolled sheet (**Papers IV, V, and VI**). The chemical compositions are given in Table 3. Test specimens have been machined using abrasive waterjet cutting.

Table 3: Chemical composition of the investigated Haynes® 282® in wt.-%.

	Ni	Cr	Co	Mo	Ti	Al	Fe	Mn	Si	C	B
Wrought bar (Paper II)	Bal	19.55	10.46	8.70	2.02	1.45	1.17	0.06	0.07	0.063	0.004
Rolled sheet (Papers IV-VI)	Bal	19.49	10.36	8.55	2.16	1.52	0.37	0.05	0.05	0.072	0.005

Waspaloy

Waspaloy is a γ' hardening nickel-based superalloy that belongs to the early generations of precipitation hardening superalloys. Its chemical composition is relatively similar to that of Haynes® 282®. Waspaloy, however, has a higher Al+Ti content. This increases the thermodynamic stability of the γ' phase. This material has been investigated in **Paper V** using a 3.15 mm (1/8 in) sheet with the chemical composition given in Table 4. The material was supplied in a mill-annealed, solutionised material condition.

Table 4: Chemical composition of the investigated Waspaloy sheet material in wt.-%.

Ni	Cr	Co	Mo	Fe	Mn	Al	Ti
Bal.	19.08	13.56	4.52	1.57	0.08	1.41	3.00
Zr	**B**	**C**	**Cu**	**P**	**S**	**Si**	
0.041	0.006	0.080	0.03	0.003	-*	0.05	

5.2. Heat treatments

Apart from the as-received material conditions, emphasis has been placed on the effect of heat treatments (HT) on microstructural development and the influence of HT on resistance towards weld cracking.

ATI 718Plus®

Cast material is typically put through a homogenisation heat treatment to level out the elemental segregation present due to the casting process. For Nb-bearing alloys the brittle Laves phase is of concern; it forms due to accumulation of Nb in the interdendritic regime during solidification. The phase is not thermodynamically stable at the nominal alloy composition and can therefore be dissolved by homogenisation heat treatments. Homogenisation heat treatments have been carried out below, at, and above the incipient Laves melting temperature of the material of 1163 °C [11]. The temperatures were chosen as 1120, 1160, and 1190 °C, with exposure times of 4 and 24 h. Note that while such homogenisation heat treatments are commonly carried out in conjunction with hot isostatic pressing (HIP) in industry to remove casting defects, a lab-scale furnace at ambient pressure was used in the present study.

Haynes® 282® and Waspaloy

In **Paper II**, heat treatments on Haynes® 282® were performed in a vacuum furnace with a heating rate of 4-11 °C/min and Ar forced convection cooling, resulting in a cooling rate of >50 °C/min. The investigated temperatures were chosen to:

- Dissolve γ' in the material at 1010 °C, based on the γ' solvus of 997 °C [106]. Exposure time was set to 1 h.
- Remove secondary $M_{23}C_6$ carbides (solvus 1019 °C) without affecting primary and M_6C carbides at 1120 °C (0.5 h exposure time). This temperature represents the lower limit of the recommended solution annealing window [107].
- Produce a coarse grained microstructure by heat treating the material at 1150 °C for 2 h.
- Age harden the material at 788 °C for 8 h.

Furnace heat treatments were used in **Papers IV-VI** to put material through an age-hardening heat treatment (**Papers IV** and **V**) and to produce a coarse-grained microstructure (**Paper VI**). Heat treatments were carried out under an Ar-protective atmosphere with a gas flow of 100 l/h. Table 5 shows the heat treatment parameters used for Haynes® 282® [99, 107] and Waspaloy [15].

Table 5: Heat treatments carried out on Haynes® 282® and Waspaloy in Papers IV-VI.

Haynes® 282® age hardening HT	1010 °C 1 h + 788 °C 8 h
Haynes® 282® coarse-grained microstructure	1150 °C 2 h
Waspaloy age hardening HT	995 °C 2 h + 845 °C 4 h + 760 °C 16 h

In **Paper IV** a test matrix was developed to study the temperature range where SAC occurs, resulting in 5 investigated temperatures (750–950 °C) and 12 exposure times (5–1800 s), as shown in Figure 10.

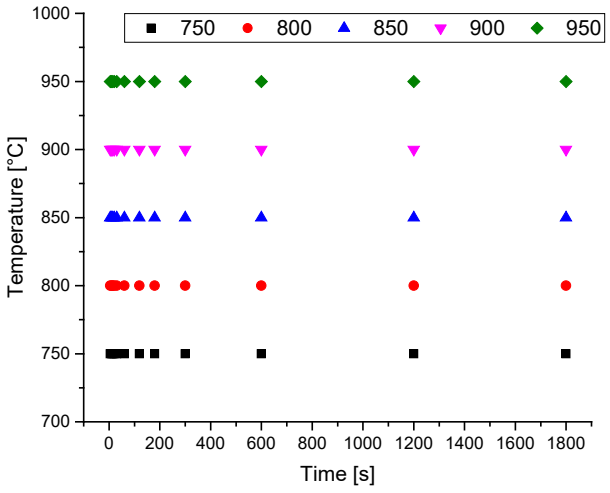

Figure 10: Temperatures and exposure times used to investigate the SAC susceptibility of Haynes® 282® [108] (Paper III).

While all following investigations used the same temperature-time parameter window, the number of studied exposure times was reduced in **Papers V and VI**.

5.3. Welding

Manual GTAW was used in **Papers II and III**. In the former, circular grooves were filled with Haynes® 282® filler wire using a tungsten-2% thorium (WT-20) electrode. Ar gas was used as a shielding gas with a nozzle gas flow of 8-15 l/min. A matching chemistry filler material in the form of 1.14 mm wire was used with negative polarity and two welding currents, 120 and 140 A. The interpass temperature was approximately 50 °C and was reached by quenching with Ar gas in between layer depositions. While the welding parameters were similar in **Paper III**, linear grooves of 30 x 10 x 10 mm and a bottom radius of 5 mm were filled using ATI 718Plus® filler wire. Figure 11 shows filled weld grooves for Haynes® 282® and cast ATI 718Plus®.

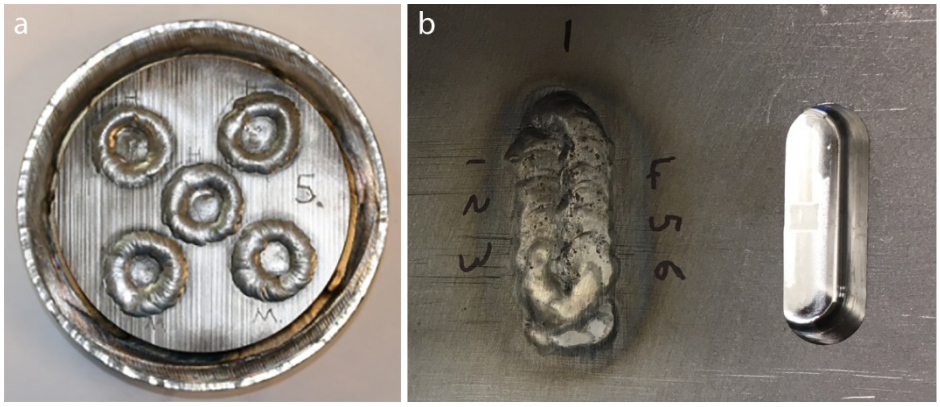

Figure 11: (a) Welded disc of Haynes® 282®, Paper II. [99]. (b) Linear groove design used in Paper III for cast ATI 718Plus®.

5.4. Gleeble testing

A Gleeble 3800 thermomechanical simulator was used in **Papers III-VI**. In **Paper III**, the heating portion of the HAZ thermal cycle was simulated to help explain the cracking behaviour in cast ATI 718Plus®. Parameters similar to those of the hot ductility test (HDT) were used [109], with a 111 °C/s heating rate and 0.03 s holding time followed by pulling samples to fracture at 55 mm/s. **Papers IV-VI** investigate the influence of exposure time on the SAC susceptibility of Haynes® 282® and Waspaloy by controlling the exposure time in the γ' precipitation temperature range. The test parameters are listed in Table 6.

Table 6: Parameters used for Gleeble testing in Papers IV-VI.

Temperature [°C]	750			800			850			900		950
Exposure time [s]	5	10	15	20	30	60	120	180	300	600	1200	1800
Heating rate [°C/s]	1000											
Cooling rate (T>500 °C) [°C/s]	100											
Stroke rate [mm/s]	0.011			0.055			0.55				55	
Chamber pressure [mbar]	0.1											
Thermocouple	Type K											

5.5. Sample preparation and investigation techniques

5.5.1. Metallographic preparation

Samples were mounted in hot mounting resin, followed by automatic grinding and polishing. For microstructural analysis, samples were electrolytically etched with 10wt.-% oxalic acid at 3V DC for 3-5 s. To analyse γ' in **Paper IV**, a second etchant was used, which removes γ' and carbides while leaving the matrix unaffected. This has been found to lead to more accurate results in image analysis [110]. The etchant consists of 50 ml 37 wt.-% HCl, 25 ml 65 wt.-% HNO_3, 2 g $CuCl_2$ and 200 ml DI H_2O. Samples were submersed for 40 s at room temperature.

5.5.2. Microstructural analysis

Microstructural characterisation was initially carried out using light optical microscopy. In the case of crack analysis, non-etched samples were used as a first step. An Olympus BX60M light optical microscope was used for all investigations. For area measurements, an Olympus SZX 9 stereo microscope was used. Selected samples were further investigated using electron microscopy, for which a Leo 1550 FEG SEM, equipped with Oxford instruments EDS and EBSD detectors, and a ZEISS Evo 50 SEM were used.

Transmission electron microscopy (TEM) was used on selected samples in **Papers III-V**. A JEOL 2100F field emission TEM with 200 kV acceleration voltage was used. Samples were analysed with selected area (SA) diffraction and TEM EDS, and images were recorded in bright and darkfield contrast. Preceding the TEM investigations, selected samples were thinned to 100 µm by manual grinding on P320 to P600 SiC grinding paper. This was followed by dimple grinding to 45–50 µm with a Gatan Model 656 dimple grinder and electropolishing in a 10:90 methanol:perchloric acid solution at −40 °C using a Struers Tenupol-3 twinjet electropolisher. Samples were polarised to 10–20 V DC, so that a current density of 0.09 A/cm^2 was obtained. The process was terminated upon hole detection by the machine, which was achieved by a laser-based system.

5.5.3. Electrolytic phase extraction

Electrolytic phase extraction was used in **Paper III** to enable the study of secondary phases present in cast ATI 718Plus® via powder X-ray diffraction (XRD). The method used here is described in ASTM E963 [111] and shown in Figure 12. Extraction was carried out by submerging a rectangular sample in a solution consisting of 100 ml HCl, 900 ml methanol and 17.6 g tartaric acid. To dissolve the matrix phase, samples were polarised to 0.1 mA/cm^2 and kept in the solution for 4 h. The extracted powder was filtrated using a 0.8 µm filter paper and dried for further analysis.

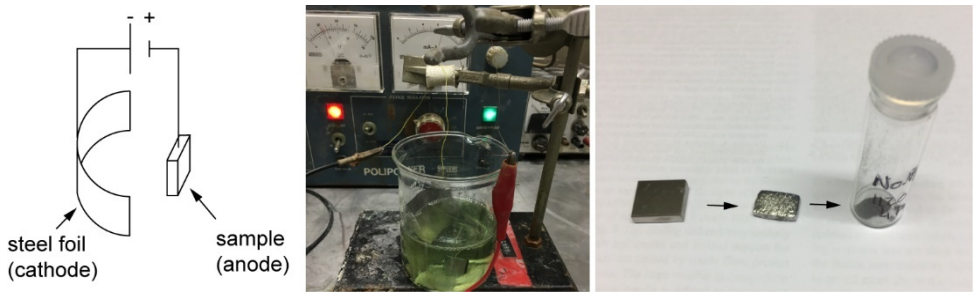

Figure 12: Experimental setup for electrolytic phase extraction from cast ATI 718Plus®.

5.5.4. X-ray diffraction (XRD) on extracted powder

A Bruker D5000 powder diffractometer was used for XRD analysis on extracted powder from cast ATI 718Plus®. The step size was 0.01°, and the holing time per step was set to 4 s. Peak analysis and indexing was carried out using the pdf 2018+ database.

5.5.5. Hardness testing

A Shimadzu HMV-2 and a Struers Durascan 70 G5 microhardness tester were used to measure Vickers hardness with a force of 0.5 kgf (HV0.5). Measured values represent the average of 5 indentations.

5.5.6. JMatPro modelling

JMatPro v.11.2 in conjunction with the nickel-based superalloy database was used to model the phase stability of the investigated alloys.

6. Summary of results and discussion

This thesis is the outcome of 4.5 years of research that led to the 6 appended papers. The results of the papers are presented here in condensed form and put into relation with the research objectives.

6.1. Microstructural characterisation

Apart from the as-received material condition, emphasis was placed on the effect that different heat treatments have on the microstructural evolution and weld cracking behaviour. The material characterisation of the investigated alloys is presented below in summarised form.

6.1.1. Cast ATI 718Plus®

Cast microstructures are heavily segregated, which is especially visible for Nb-bearing nickel-based superalloys. In those alloys, the Laves phase forms as a terminal solidification product due to Nb-segregation in the melt. Furthermore, Nb-rich MC-type carbides are typically present. The high Nb-content of secondary phases present in interdendritic areas produces a strong elemental contrast in SEM BSD images, as shown in Figure 13 b.

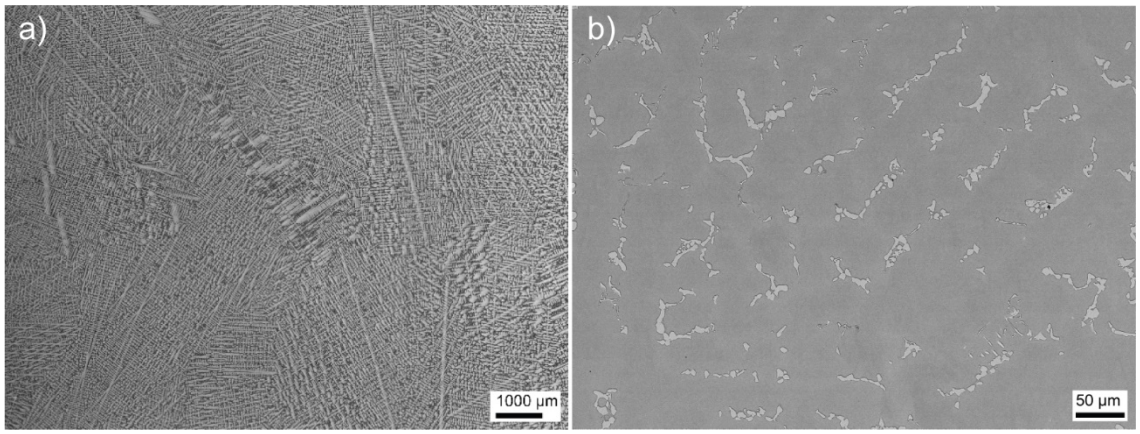

Figure 13: As-cast microstructure of ATI 718Plus®, with the large grain structure visible in (a) and Nb-rich precipitates in interdendritic regions shown in SEM BSD contrast (b) [45].

The phases present in the as-cast microstructure of ATI 718Plus® were identified as Laves phase, Nb-rich MC-type carbides and γ' by the use of transmission electron microscopy. Figure 14 exemplarily shows TEM results confirming the presence of Laves phase via TEM EDS and SA diffraction analysis.

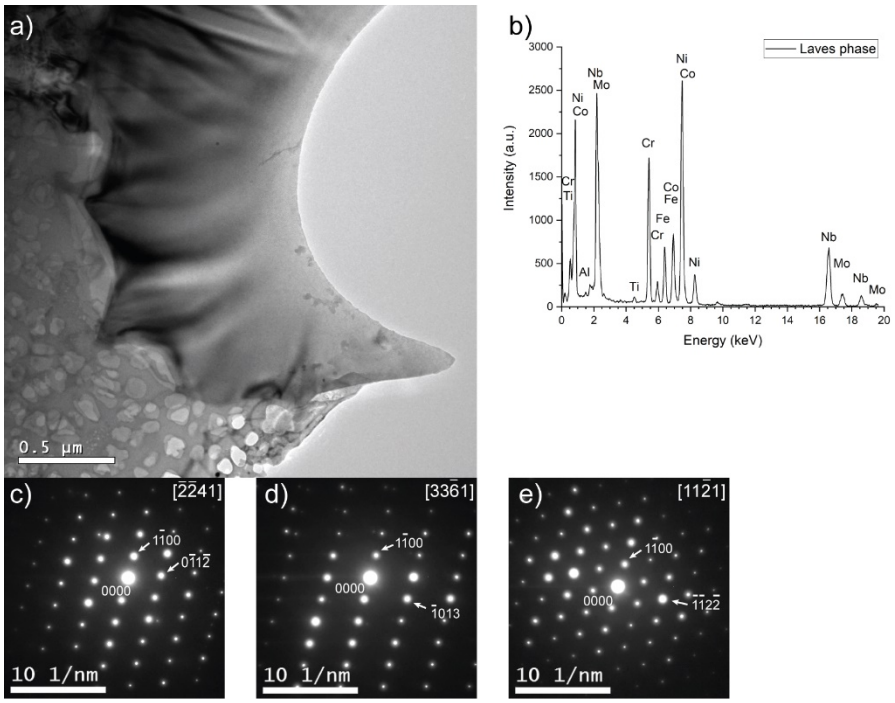

Figure 14: TEM brightfield image of Laves phase in as-cast ATI 718Plus® (a). TEM EDS results are in (b), while SA diffraction patterns show a hexagonal P63/mmc structure with $[\bar{2}\bar{2}41]$ (c), $[33\bar{6}1]$ (d) and $[11\bar{2}1]$ (e) [45].

Homogenisation heat treatments are used to dissolve the Laves phase, which is not thermodynamically stable at the nominal alloy composition. It was, however, found that a significant amount of Nb-rich phases remained in the microstructure after the 1120 °C 4-h heat treatment. The efficacy of the homogenisation heat treatments can be seen in Figure 15. The XRD analysis performed on electrolytically extracted powder shown here confirms the dissolution of the Laves phase for the 1190 °C 24-h heat treatment, whereas Laves peaks are still present for samples heat treated at 1120 °C for 4 h.

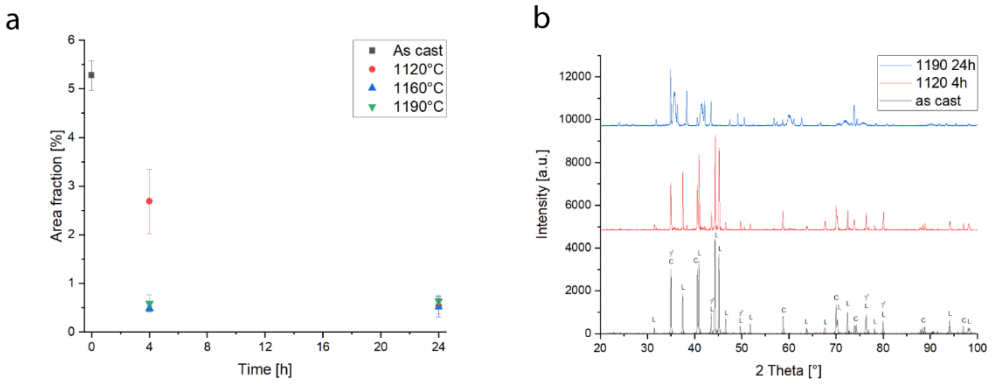

Figure 15: (a) Area fraction of Nb-rich precipitates for different heat treatments and exposure times. (b) XRD spectrum from electrolytically extracted powder of cast ATI 718Plus®, with as-cast (bottom) and 1120 °C 4 h (middle) showing Laves phase peaks in contrast to 1190 °C 24 h (top) [45].

6.1.2. Haynes® 282®

A typical as-received microstructure of a Haynes® 282® forged bar studied in **Paper II** is shown in Figure 16 (a), while Figure 16 (b) shows a sample prepared from sheet metal (**Papers IV-VI**). The grain size of both material conditions is comparable at 55 ± 5 and 51 ± 7 µm, respectively. In both materials, primary MC-type carbides are present in the form of stringers.

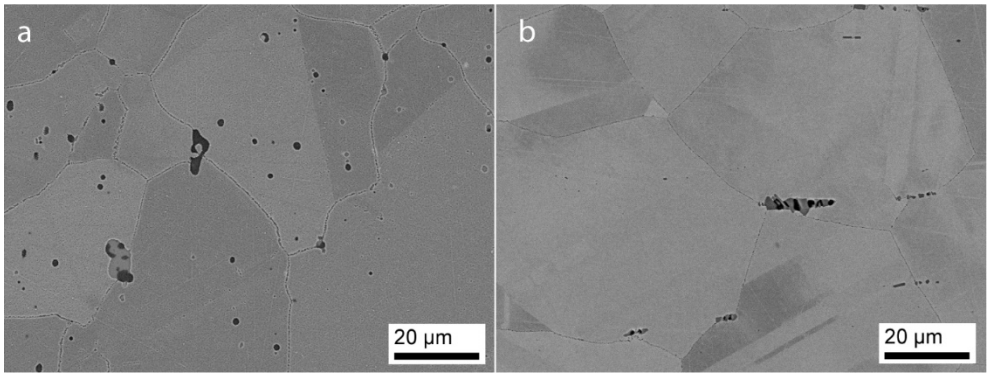

Figure 16: Microstructure of Haynes® 282® in the as-received condition of a forged bar (Paper II) (a) and sheet metal (b) (Papers IV-VI).

The as-received Haynes® 282® sheet material has a hardness of 265 ± 3 HV, which is higher than expected for a fully solutionised, γ'-free microstructure. The presence of 2.2 ± 0.4 nm diameter γ' was confirmed using TEM selected area (SA) diffraction analysis. Figure 17 shows a TEM darkfield image where γ' precipitates are visible as bright spots. The corresponding SA diffraction pattern in Figure 17 (b) clearly shows the presence of γ' sublattice reflections.

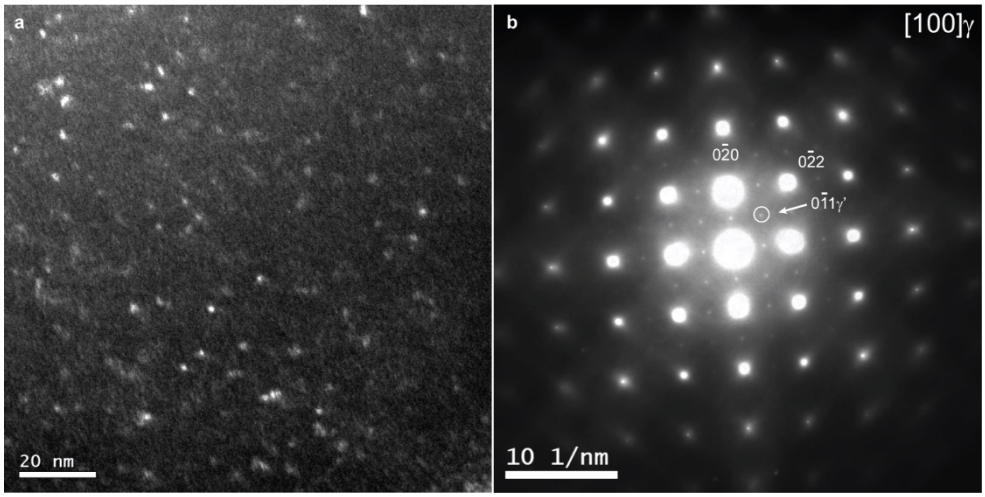

Figure 17: (a) TEM darkfield image using the <0-11> γ' diffraction spot on the gamma [100] zone axis as indicated in (b) [108] (Paper IV).

The presence of γ' can be related to precipitation reactions occurring during cooling from solution heat treatment. Forged bar specimens (**Paper II**) exhibit even slower cooling after heat treatment, resulting in higher hardness of 315 ± 7 HV.

Various heat treatments were performed on Haynes® 282® to investigate the effect of microstructural evolution on weld cracking resistance. No significant distinction can be made based on hardness when comparing a forged bar (375 ± 5 HV, averaged over all age hardened discs) and sheet material (380 ± 5 HV) after a conventional two-step age hardening heat treatment. The heat treatment produced a distinct grain boundary carbide network. Secondary carbides present in the material were identified as Mo-rich M_6C and Cr-rich $M_{23}C_6$ (**Paper IV**). The age hardening heat treatment produced γ' precipitates with an average diameter of 18.4 ± 3 nm. The presence of a grain boundary carbide network and γ' precipitates after conventional age hardening is shown in Figure 18.

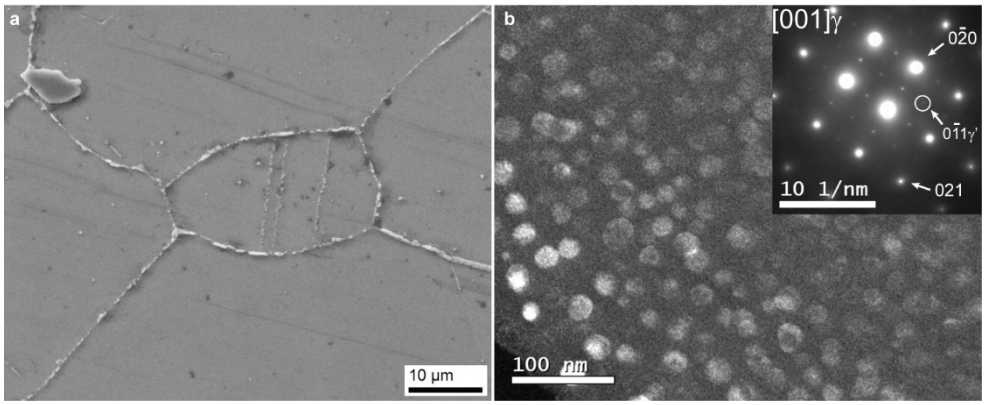

Figure 18: (a) Grain boundary carbide network in Haynes® 282® after a conventional 2-step age hardening heat treatment. (b) Fine γ' precipitates with 18.4 ± 3 nm diameter in TEM darkfield contrast using the <0-11> γ' diffraction spot on the gamma [001] zone axis [108] (PAPER IV).

Apart from the formation of grain boundary carbide networks and changes in hardness due to γ' precipitation, it was attempted to produce large grain size via heat treatment at the upper limit of the solutionising temperature window. The heat treatment at 1150 °C for 2 h led to significant grain growth in both the forged bar and sheet material, as shown in Figure 19. An approximately fourfold increase in grain size was observed for the sheet material, and grain growth was even more pronounced for the forged bar. It is noteworthy that the latter showed a wider variation in grain size, which may be related to the less uniform microstructure along the diameters of the forged discs as compared to the sheet metal, for which more uniform material conditions can be assumed.

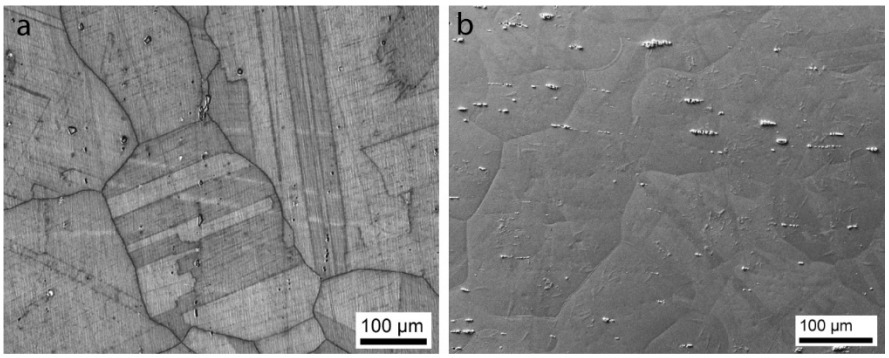

Figure 19: Large grain size in Haynes® 282® after heat treatment at 1150 °C for 2 h; forged bar (a) (Paper II) and rolled sheet (b) (PAPER VI) [99, 108].

Haynes® 282® has a reported γ' solvus of 997 °C [106], and thus precipitation and coarsening reactions are expected when heat treating the material in the temperature range of 750–950 °C (**Papers IV-VI**). The presence of fine γ' in the as-received material makes it likely that particle growth is the dominating mechanism. Particle size evolution follows the Lifshitz-Slyozov-Wagner (LSW) theory as shown in Figure 20, supporting this hypothesis.

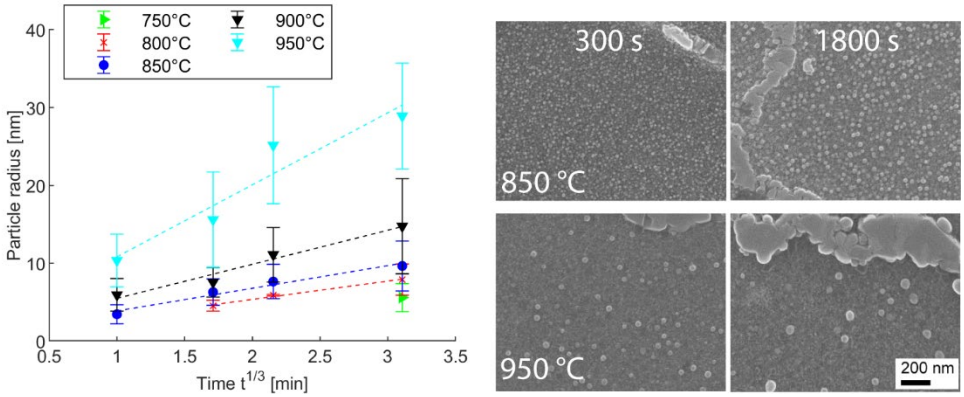

Figure 20: Average γ' particle radius after isothermal exposure. LSW fit is indicated by dashed lines. Also shown are microstructure images taken after 300 and 1800 s thermal exposures at 850 and 950 °C. Adapted from [108] (PAPER IV).

The γ' precipitation led to a significant hardness increase for all investigated temperatures. The relatively short exposure time of 1800 s was able to increase the hardness to 367 ± 5 HV, which is close to the hardness achieved by a conventional age hardening heat treatment. The hardness evolution is shown in Figure 21 and is in good agreement with data found in the literature [112–114].

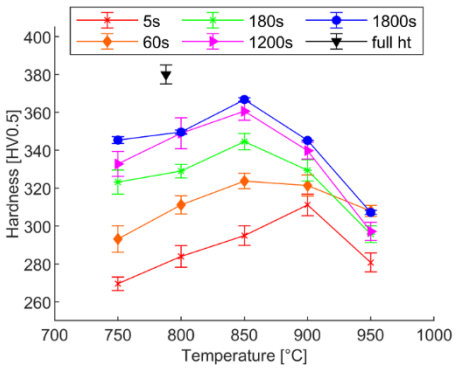

Figure 21: Hardness of Haynes® 282® after isothermal exposure. Hardness for conventionally age hardened material is included to show the progress of the age hardening during short thermal exposure [108] (PAPER IV).

The hardness of the material with large grain size was not significantly affected for the forged bar, but lower values were observed for the sheet material. Hardness in Haynes® 282® is mainly affected by the presence of the γ' phase [114]. Some contribution of grain size can, however, be expected, and it is described by the Hall-Petch relationship:

$$\sigma_y = \frac{\kappa}{D^{0.5}}, \tag{2}$$

where κ is the Hall-Petch slope and D is the grain size. Using data for κ from [115], it becomes clear that the effect of grain size on the material's hardness is low. This is further supported by the insignificant hardness change in the forged bar material, leaving changed γ' precipitation and growth conditions as reasons for the lower hardness. More rapid cooling after the heat treatment is hence the most likely explanation.

Haynes® 282® forms secondary $M_{23}C_6$ and M_6C carbides during heat treatment at 750–950 °C [108, 112]. While some M_6C carbides are already present in the microstructure, isothermal exposure produces a continuous grain boundary carbide network in the material. This is evident in Figure 22, which shows grain boundary carbide evolution as a function of temperature and exposure time.

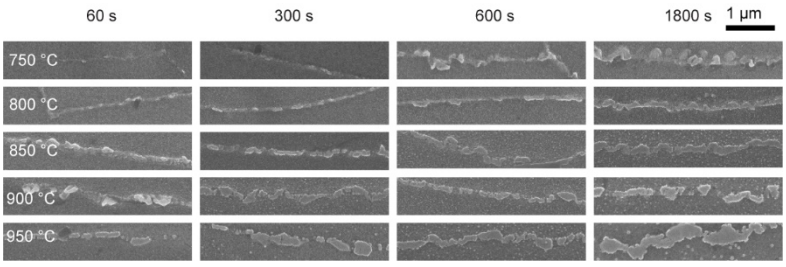

Figure 22: Grain boundary carbide network evolution in Haynes® 282® [108] (PAPER IV).

6.1.3. Waspaloy

Waspaloy has an as-received microstructure that, similar to Haynes® 282®, contains fine γ' that has precipitated during cooling in the mill-annealing process. The higher content of Al+Ti in Waspaloy stabilises the γ' phase and results in faster precipitation kinetics as compared to Haynes® 282®. The microstructure of Waspaloy in the as-received condition is shown in Figure 23 (a), while the presence of fine γ' is visible in Figure 23 (b).

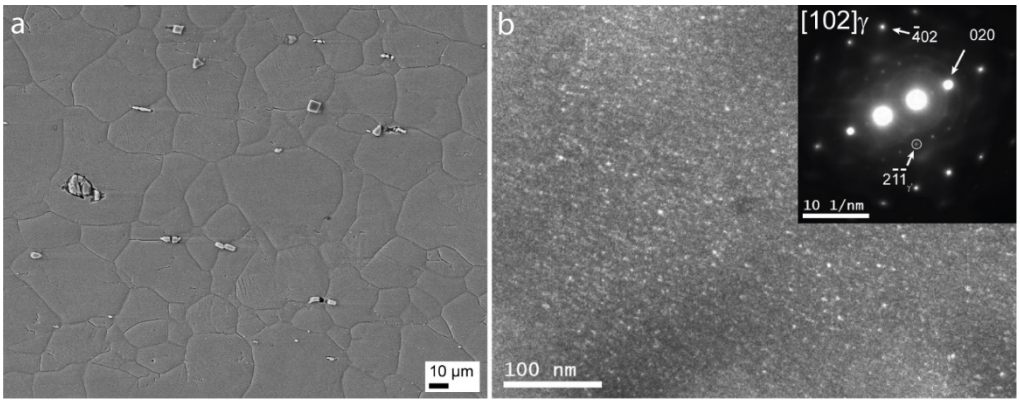

Figure 23: (a) Microstructure of as-received Waspaloy sheet material. (b) TEM darkfield image using the <2-1-1> γ' diffraction spot on the gamma [102] zone axis. γ' precipitates are visible as bright spots [116].

A conventional age hardening heat treatment that includes three temperature steps for Waspaloy leads to the microstructure shown in Figure 24. The first aging step at 996 °C causes the formation of coarse γ' in the material. No carbide precipitation occurs here since the solution temperature of $M_{23}C_6$ carbides is 965 °C [116]. During the subsequent steps a discrete network of $M_{23}C_6$ carbides and coarse γ' is formed on the grain boundaries while a bimodal γ' distribution develops. The γ' particle sizes are 133 ± 34 nm and 34 ± 7 nm, with the hardness being increased to 411 ± 3 HV0.5.

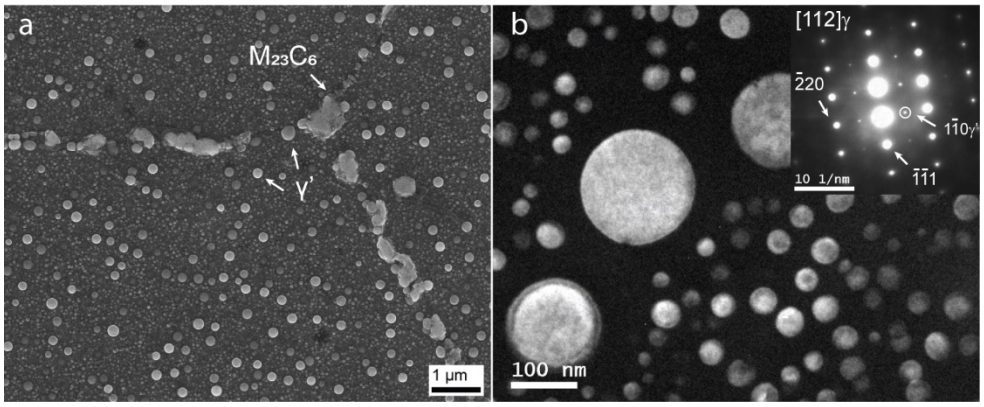

Figure 24: (a) Waspaloy after conventional three-step age hardening heat treatment. (b) γ' precipitates visible in TEM darkfield contrast using the <1-10> γ' diffraction spot on the gamma [112] zone axis [116].

Isothermal exposure in the 750–950 °C temperature range led to γ' evolution following a $t^{1/3}$ relationship (LSW theory). This is in good agreement with the literature data [117]. In contrast to Haynes® 282®, the development of a grain boundary carbide network is not as pronounced. At 950 °C only a few carbides are present owing to the close proximity to the carbide solvus temperature. While a continuous network was formed at 800 and 850 °C within 1800 s, isothermal exposure at 50 °C only resulted in minor carbide formation. Thermodynamic simulations with JMatPro show a clear difference in carbide precipitation kinetics for Waspaloy and Haynes® 282®. The latter furthermore contains two carbide species, which increases the total carbide phase fraction and explains the difference in microstructural evolution between the two alloys.

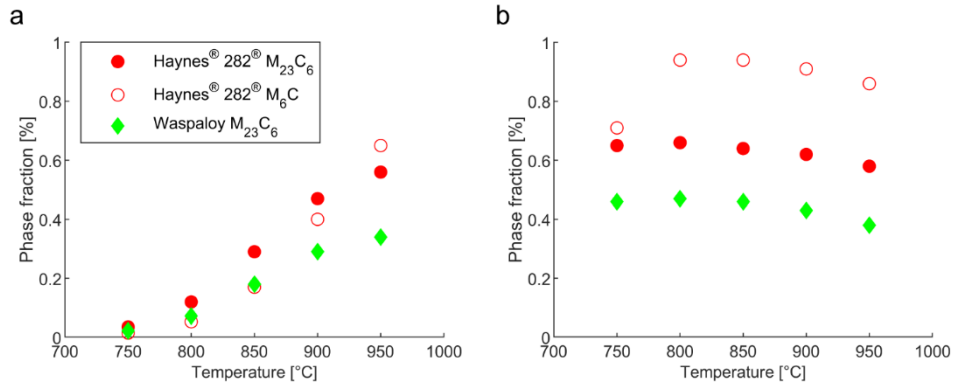

Figure 25: Secondary carbide phase fractions for Haynes® 282® and Waspaloy as a function of temperature for 1800 s (a) and 100000 s (b) [116] (PAPER V).

In contrast to the carbide precipitation kinetics, the higher Al+Ti content of Waspaloy (4.5 vs. 3.6 wt.-%) results in a higher phase fraction and more rapid precipitation of the γ' phase. This is reflected by hardness measurements as shown in Figure 26 in the form of time-temperature-hardness (TTH) diagrams.

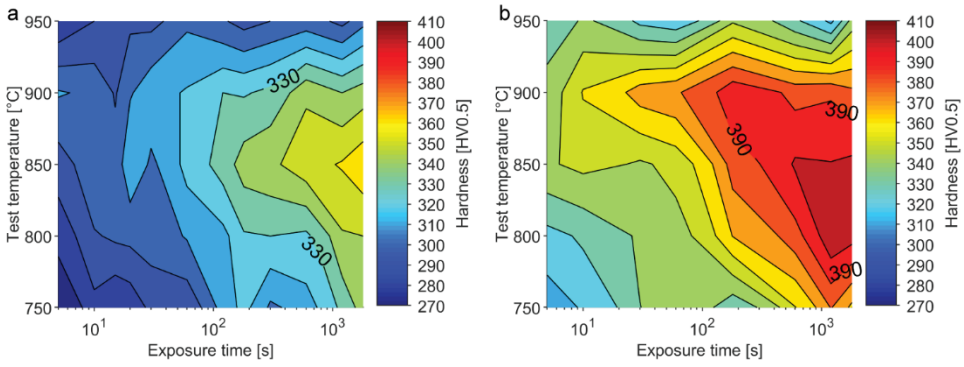

Figure 26: TTH diagrams for Haynes® 282® (a) and Waspaloy (b) for exposure times up to 1800 s. Contour spacing 10 HV [116] (PAPER V).

6.2. Repair welding characteristics of cast ATI 718Plus® and wrought Haynes® 282®

Representative weldability testing can provide a realistic benchmark of the materials' weld cracking resistance. The results of repair welding trials are presented here for cast ATI 718Plus® (**Paper III**) and wrought Haynes® 282® (**Paper II**) and are related to **Research Objective I**.

While solidification cracking was found in the fusion zone layers of cast ATI 718Plus®, the dominant cracking mechanism is HAZ cracking. Measured total crack length was higher in the base metal HAZ as compared to the FZ. The difference is even more pronounced when taking the investigated cross-sectional area into account, which was 3:1 for FZ vs. HAZ. Furthermore, an effect of pre-weld microstructure on weld cracking is observed for the HAZ. As-cast microstructure and the 1120 °C 4-h treatment showed the lowest total crack length (TCL), as indicated in Figure 27 (a). The difference becomes more evident when comparing the average crack length (Figure 27 (b)), which is significantly lower for those material conditions.

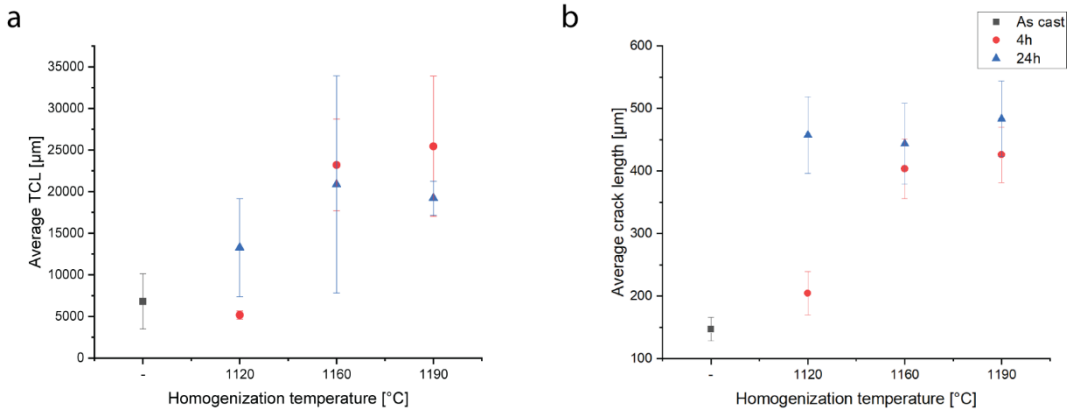

Figure 27: Total crack length (a) and average crack length (b), measured in the base metal HAZ as a function of heat treatment condition [45] (PAPER III).

The main difference between the homogenisation heat treatments investigated in this study is their ability to dissolve the Laves phase. Short, disconnected cracks were formed in interdendritic areas when Laves phase was present in the microstructure. Homogenisation heat treatments that dissolved the Laves phase instead produced long cracks on former solidification grain boundaries. This is apparent in Figure 28, where the different crack appearances for as-cast and the 1190 °C 24-h homogenised condition are shown.

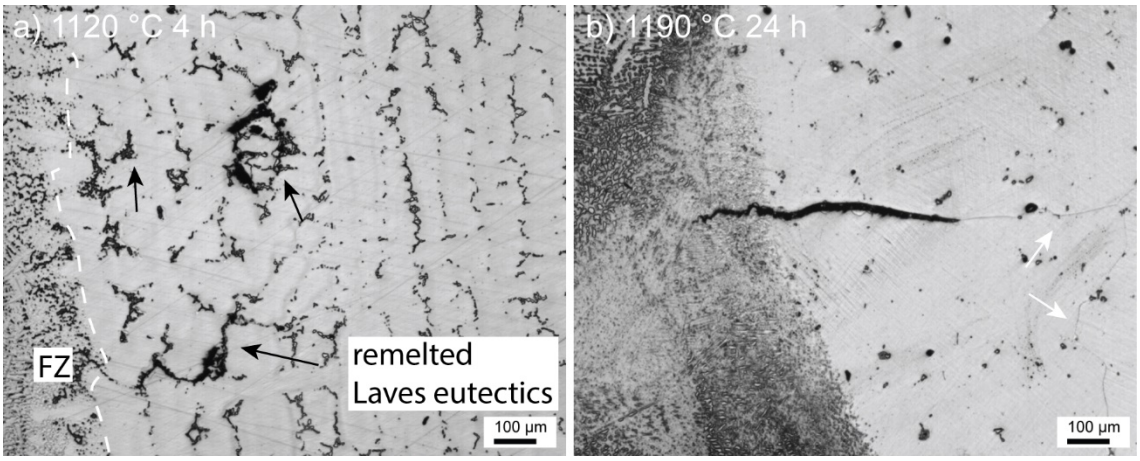

Figure 28: Crack appearance in base metal HAZ of (a) as-cast material and (b) 1190 °C 24-h homogenised condition. Note melted gamma-Laves eutectics as indicated by black arrows. White arrows point to crack locations on solidification grain boundary [45] (PAPER III).

Based on these observations a liquation mechanism for HAZ cracking has been proposed. In Laves-free microstructures, constitutional liquation of Nb-rich MC-type carbides is found to contribute to the formation of liquid on solidification grain boundaries. Otherwise liquid is assumed to form by matrix melting, with a possible effect of boron segregation. Liquid formed on solidification grain boundaries can spread over a wide area, lowering the load bearing capabilities of the material. The abundance of Laves phase in the as-cast and 1120 °C 4-h material condition produced a large amount of liquid during welding due to gamma-Laves eutectic melting. A high amount of liquation has been found to lower cracking [88], which can be rationalised by applying Borland's generalised theory and Pellini's theory of hot tearing [21, 22]. The availability of large amounts of liquid enables greater mobility of the remaining solid matrix phase and can thus help to accommodate stresses generated from the weld thermal cycle.

Repair welding of Haynes® 282® showed that regardless of the welding parameters applied in the study (with 120 A welding current being typical welding conditions and 140 A representing a more severe environment), no cracks were present in the base metal HAZ. Instead, all cracking was confined to the FZ. No correlation between base metal heat treatment history and cracking response could be observed. The cracking response was instead strongly influenced by the heat input, with the use of 140 A welding current leading to 1.5× more cracks in the weld deposit layers, as visible in Figure 29.

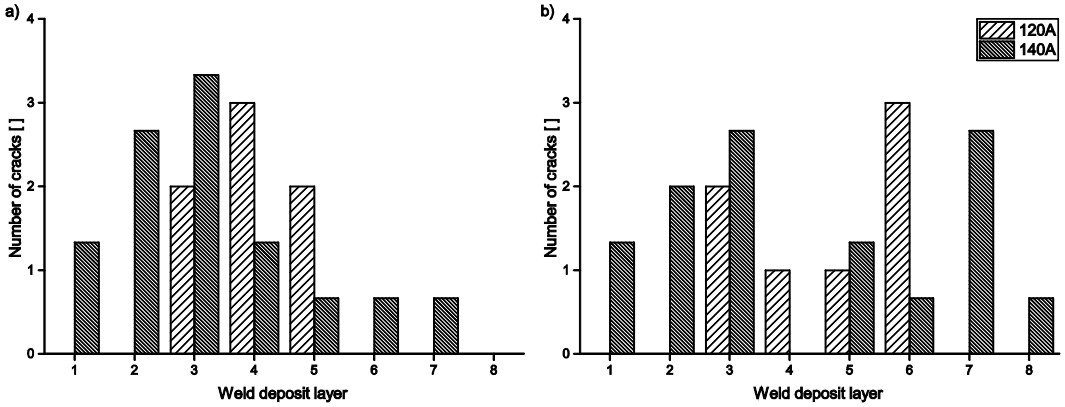

Figure 29: Total number of cracks per weld deposit layer. (a) Pre-weld heat-treated discs (1-4). (b) Pre + post-weld heat treated discs (5-8). Results for 140 A are normalised to account for differences in sampling size for the two conditions [99] (PAPER II).

Furthermore, it can be observed that the cracking response is independent of both the pre-weld microstructure and PWHTs (cf. total number of cracks in Figure 29 (a) and (b)). Supported by microstructural analysis showing a dendritic structure on the crack surfaces and the location on solidification grain boundaries, the cracks were classified as solidification cracks. Small voids without signs of liquid phases being present were also found in the FZ layers. These voids were initially considered to be potential SAC. The EDS analysis, however, revealed the presence of aluminium-rich oxides. This led to the assumption that the voids are in fact related to oxide layers present from the welding process that have not been properly removed, cf. Figure 30.

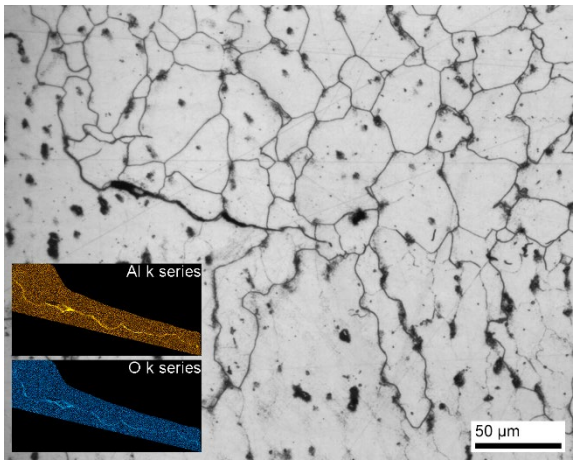

Figure 30: Aluminium-rich oxide layer and a presumed start location (140 A welding current) [99] (PAPER II).

Hardness measurements in both FZ layers and base metal HAZ revealed that 3-4 weld deposit layers are necessary for the hardness to exceed 300 HV in the weld metal. The HAZ showed the same trend, but a slightly quicker hardening response, with only two weld deposit layers being required to reach this hardness level. The absence of SAC in the material suggests that either the weld residual stresses were below a critical level or that the hardening response was too slow for SAC to occur in the

material. This indicates that SAC is not a major concern and that instead, solidification cracking should be expected when welding Haynes® 282®. This is a good sign for the application of the alloy as a supplement for Alloy 718. Nevertheless, the mechanism of SAC and the resistance of candidate alloys for future application in the aero engine sector need to be further investigated. While showing the material's weldability under realistic conditions when carrying out repair welding studies, a test setup that also enables a higher degree of control over test parameters, such as stress and temperature, is needed to understand the underlying mechanisms and to provide a more reliable statement about the SAC susceptibility of Haynes® 282®.

The repair welding characteristics of cast ATI 718Plus® and wrought Haynes® 282® can be summarised as follows:

- HAZ cracking is the dominant weld cracking mechanism in cast ATI 718Plus®;
- Laves phase can be removed by homogenisation heat treatments;
- HAZ cracking in cast ATI 718Plus® is correlated with the amount of Laves phase;
- Laves phase reduces HAZ cracking due to the formation of large amounts of liquid in the HAZ;
- Haynes® 282® shows generally good weldability, with only solidification cracks found in the fusion zone of multi-pass welds;
- No cracks were found in the base metal HAZ, irrespective of base metal microstructure; and
- The results suggest that the hardening response of the material is too slow to cause SAC in conjunction with the weld residual stresses present in the studied setup.

6.3. Development of a testing procedure to investigate the SAC mechanism

For new alloys in particular, welding trials can provide a useful impression of the actual welding response of the material, which can then be used for further, more controlled studies. Screening tests are important for investigating the relative resistance of different alloys towards SAC. **Paper I** reviewed the literature to identify the underlying mechanisms and influencing factors of SAC, which have been presented in abbreviated form in the introduction part of this thesis. A review of the research on SAC over the years indicates that while initial investigations focused on the general mechanism, more novel research has focused on the development of testing procedures using modern equipment and the investigation of new alloys. Another part of **Paper I** was the evaluation of the test methods available for assessing susceptibility towards SAC. It was found that several methods have been developed over the years, although none of them is able to address all aspects of SAC. Tests measuring ductility were found to be the most promising approach [76].

To study the effect of microstructure on SAC susceptibility **(Research Objective II)**, a test that enables the study of short exposure times in the SAC temperature range is necessary to consider the rapid precipitation of the γ' phase in SAC susceptible materials. The microstructural component of strain age cracking is composed of the effect of hardening precipitates (γ') and the condition of grain boundaries where stresses are localised. Using a Gleeble system enables precise control of the thermal cycle, combined with the ability to rapidly deform material; a Gleeble system was thus chosen to carry out the experiments. The general observation from the constant heating rate test (CHRT), that is, the loss of ductility in the intermediate temperature range, was taken as a starting point for the test design. As the loss in ductility is less severe for alloys with a reduced amount of hardening elements, such as Al and Ti, the susceptibility to SAC strongly depends on alloy composition [19, 118, 119]. Based on that, an interrelationship of ductility and precipitation kinetics has been proposed [70], but no quantified data is available yet.

Since the CHRT uses a constant heating rate to reach the different test temperatures, the effect of hardening reactions cannot be investigated as exposure time is not a controlled parameter. The new approach instead utilises fast heating of 1000 °C/s and subsequent isothermal exposure to obtain microstructures with varying precipitation structure. The test temperatures were selected based on the results of a previous CHRT investigation such that the test covers the temperature range around the drop in ductility [19]. In the CHRT, the total exposure time in the precipitation temperature range is 20-30 min, including both the heating and mechanical testing parts of the test [118, 119]. Hence, the two longest exposure times in the new approach were considered to reflect conditions comparable to those of the CHRT. The Gleeble system utilises resistance heating to achieve rapid temperature changes. With water-cooled grips, this results in a parabola-shed temperature distribution along the specimen axis. When testing at elevated temperatures, such a non-uniform temperature distribution is not a problem and is in fact beneficial if the steep thermal gradients present in weld heat-affected zones are to be simulated. When testing precipitation hardening superalloys in the temperature range where age hardening reactions occur, such a setup can, however, cause problems. The γ' precipitation occurring in the sample centre can cause increased strength relative to the colder, not hardened parts of the specimen. The problem has previously been recognised, and two approaches have been applied as a solution. Norton and Lippold used steel jaws that reduced heat conduction as compared to the standard copper ones. Test samples then show a more uniform temperature distribution, preventing off-centre fractures [120]. A narrower high-temperature zone enables faster temperature control, and thus this work followed the approach taken by Metzler, who used a radius, instead of a constant gauge width, to compensate for lower strength along the specimen axis [119]. Finite element simulations

show the effect of specimen geometry on the failure location, as shown in the results from **Paper IV** presented in Figure 31.

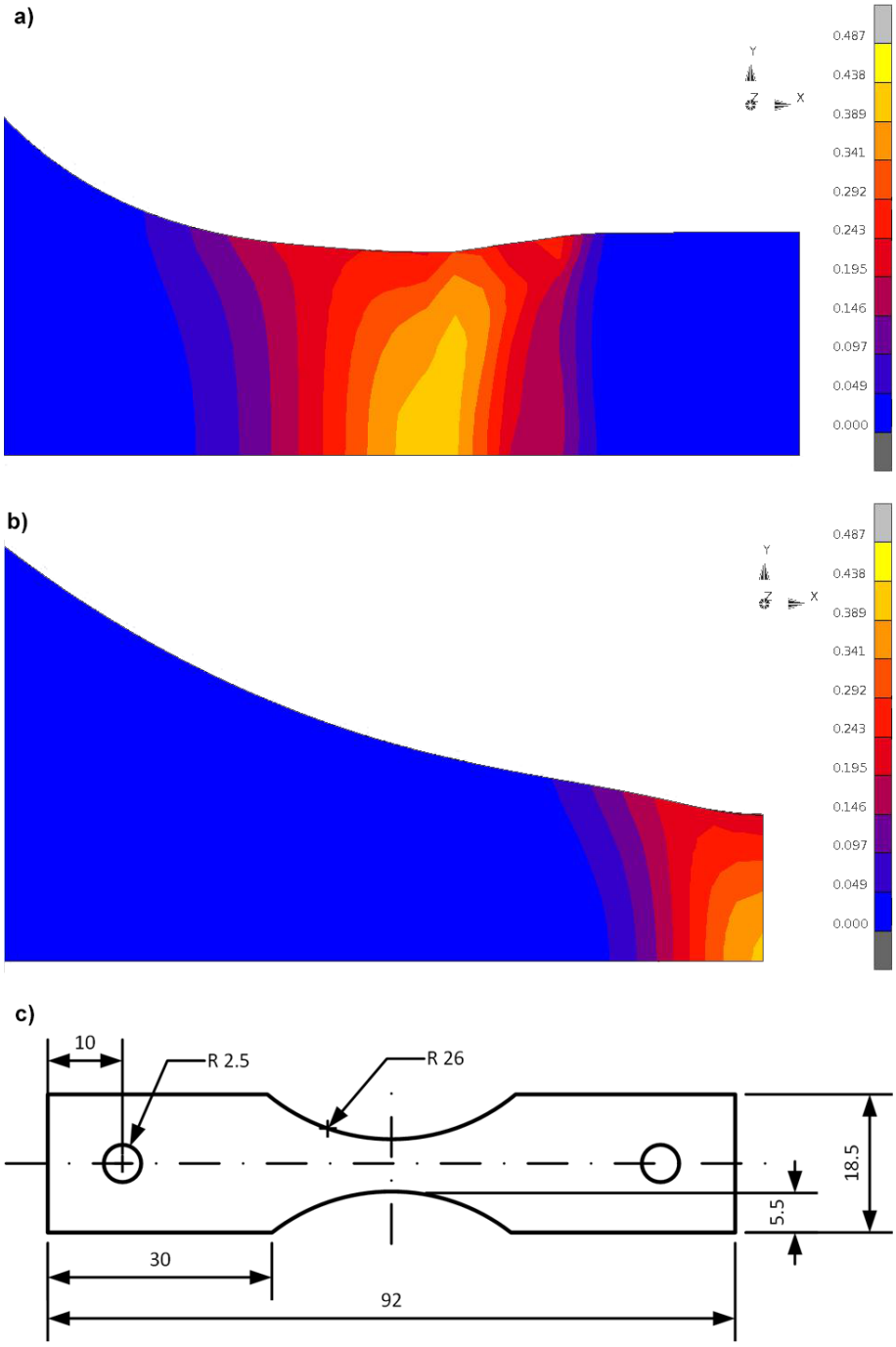

Figure 31 Simulated total equivalent plastic strain for a specimen with constant gauge length (a) and 26 mm radius (b). Optimised specimen geometry is shown in (c) [108].

6.4. The effect of microstructure on SAC

The short thermal exposure studied (5-1800 s) caused significant changes in the microstructure as shown in the previous chapter. The correlation between the microstructural evolution and the ductility of Haynes® 282® and Waspaloy has been investigated in **Papers IV-VI**. It was found that the fracture mode in the investigated temperature range is dependent on the rate of deformation. Intergranular fracture, which is characteristic of SAC, was only found when stroke rates were sufficiently low. High stroke rates, on the other hand, resulted in grain rupture, as shown in Figure 32.

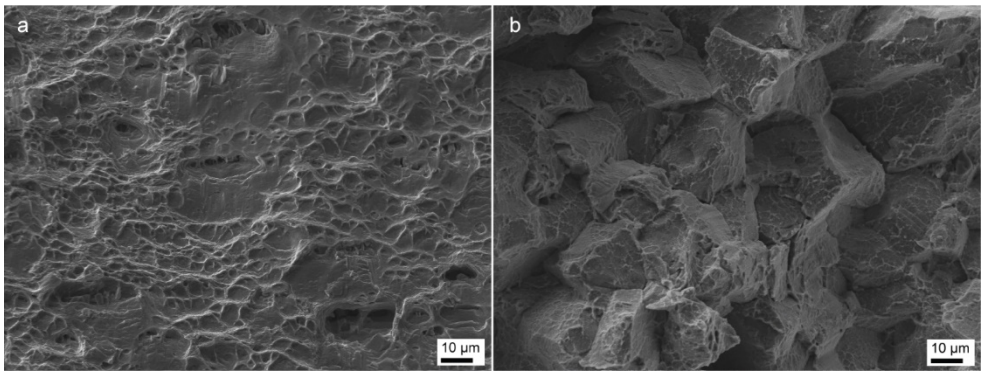

Figure 32 Fracture surfaces of Waspaloy for fast (55 mm/s) and slow (0.055 mm/s) stroke rates, showing grain rupture and intergranular fracture, respectively [116] (Paper V).

Contrary to expectation, the ductility of Haynes® 282® is not affected by ongoing hardening reactions, as similar values were obtained for both the 120 and 1800 s exposure times in the lower range of the investigated temperature window. While hardness increased significantly during thermal exposure, an effect was only seen when deformation was characterised by grain rupture (i.e. for high deformation rates). Figure 33 presents the ductility of Haynes® 282® as a function of temperature and exposure time for 55 mm/s (a) and 0.055 mm/s (b). It is apparent that a direct effect of γ' precipitation is only present if grain rupture is the dominating fracture mode (fast stroke rates). If deformation is localised onto the grain boundaries, no clear change in ductility can be observed over the investigated exposure time range.

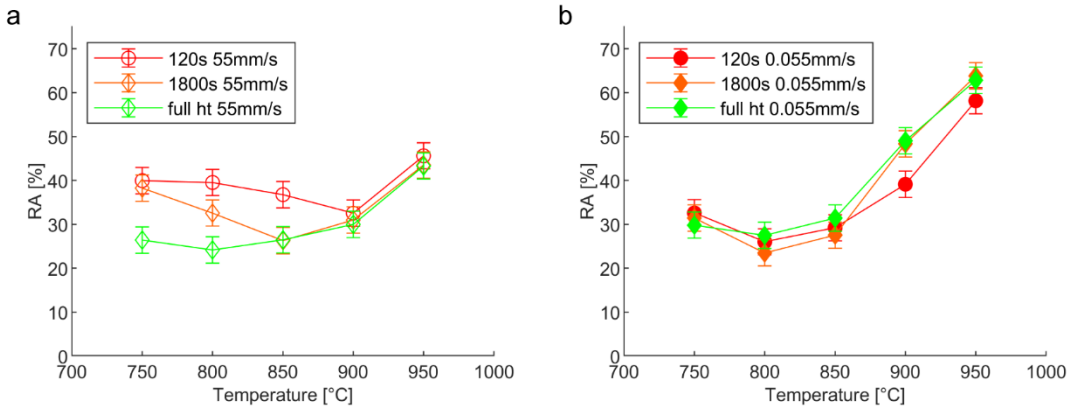

Figure 33: Ductility of Haynes® 282® as a function of temperature for different exposure times for (a) 55 mm/s and (b) 0.055 mm/s stroke rate.

Waspaloy, on the other hand, does show a decrease in ductility when comparing 120 s and 1800 s exposure times, cf. Figure 34.

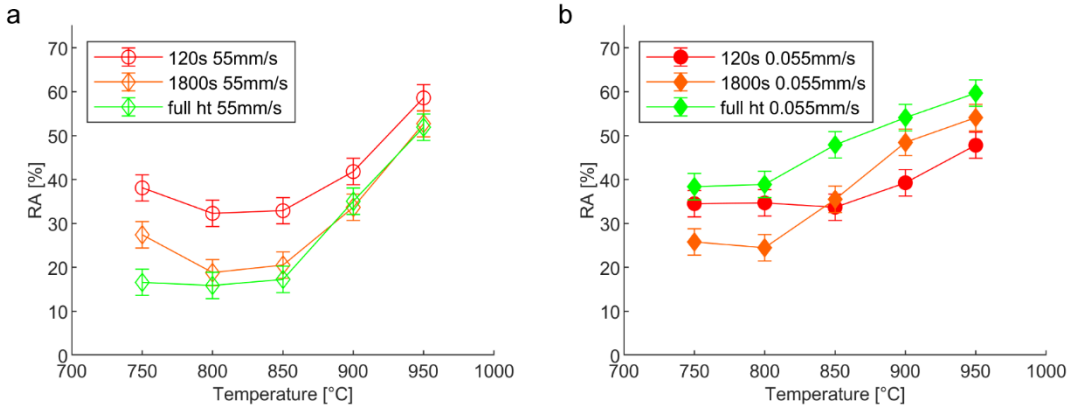

Figure 34: Ductility of Waspaloy as a function of temperature for different exposure times for (a) 55 mm/s and (b) 0.055 mm/s stroke rate [116].

At the same time, a conventional heat treatment led to higher ductility. This is noteworthy as this material condition also shows the highest hardness. While a very similar age hardening effect is observable even after 1800 s isothermal exposure, the major difference in microstructure is the presence of a continuous grain boundary precipitate network consisting of discrete carbide and γ' particles in conventionally aged Waspaloy. Thermal exposure in the temperature range where the ductility minimum occurs led to the formation of grain boundary carbide networks; however, the amount of precipitates on the grain boundaries is reduced, and no discrete particle morphology is observable.

The ductility response of Waspaloy helps to explain the ductility response of Haynes® 282®, as the latter has a higher phase fraction of secondary carbides (cf. Figure 25), which increases the strengthening effect on the grain boundaries. This appears to be sufficient to offset the effect of the more moderate hardness increase Haynes® 282® has as compared to Waspaloy.

The comparatively high ductility measured for Waspaloy is unexpected considering the reportedly higher SAC susceptibility of the material. A possible explanation is the smaller grain size of Waspaloy, which is approximately 50% of that of Haynes® 282® (24 ± 5 vs. 55 ± 5 µm).

Grain size is generally considered to have a negative effect on SAC susceptibility due to the concentration of stresses onto a smaller grain boundary area [79, 81]. The effect of grain size is clearly observable for Haynes® 282®, where a fourfold increase in grain size after heat treatment at 1150 °C for 2 h not only widened the temperature range in which low ductility occurs but also decreased the ductility in general, as shown in Figure 35 (cf. Figure 33 (b)).

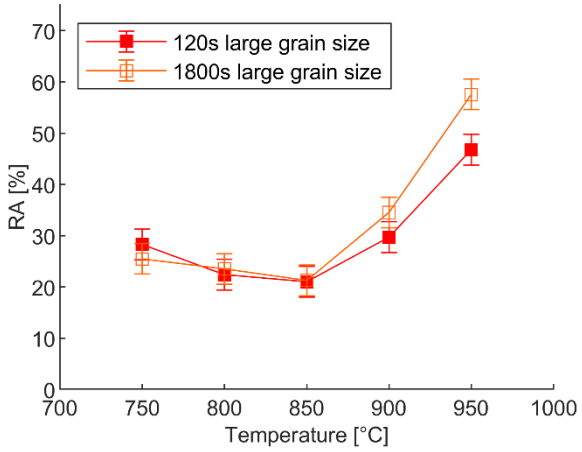

Figure 35: Ductility as a function of temperature for large grain size Haynes® 282® [121] (Paper VI).

Considering the combined results of **Papers IV-VI**, the effect of microstructural evolution on the ductility of Haynes® 282® can be understood as the combined effect of the rapid formation of a grain boundary carbide network and a moderate hardness increase due to γ' precipitation. This is in contrast to Waspaloy, for which a lower amount of grain boundary precipitates cannot compensate for the more rapid γ' precipitation and the resulting grain interior hardening. Grain size has a significant effect on the ductility response and should be kept small to increase the material's ductility.

7. Conclusions

The weld cracking behaviour of precipitation hardening nickel-based superalloys has been investigated in this thesis by means of repair welding trials and the development of a simulative test procedure using a Gleeble system. The conclusions are grouped into two categories based on the research questions:

Effect of microstructural evolution on weld cracking during repair welding operations (RQ 1 and 2)

- The efficiency of homogenisation heat treatments of cast ATI 718Plus® to dissolve Laves phase was investigated using advanced microstructural characterisation. Incomplete Laves phase dissolution has been correlated with increased resistance towards HAZ liquation cracking. The presence of Laves phase provides large amounts of liquid during the weld thermal cycle, which has been connected to an increased capability of the material to relax weld thermal stresses.

- Haynes® 282® shows good resistance towards HAZ cracking, while the observed solidification cracking was found to be dependent on the welding parameters, such as heat input. Post-weld heat treatments did not cause strain age cracking in the material, indicating good resistance of Haynes® 282® towards this cracking phenomenon.

The developed Gleeble-based simulative test procedure enabled investigation of the effect of rapid microstructural changes, such as γ' precipitation, on strain age cracking of Haynes® 282® (RQ 3 and 4)

- The ductility response of Haynes® 282® and hence its SAC susceptibility is largely independent of heat treatment. The rapid formation of a grain boundary carbide network has been found to counter the effect of the age hardening of the grain interior due to γ' precipitation.

- Key components of the SAC mechanism have been identified as γ' precipitation, grain boundary strengthening by secondary carbides, and grain size. The combination of the moderate age hardening kinetics in Haynes® 282® combined with the rapid formation of a grain boundary carbide network have been identified as a main reason for the material's good resistance towards SAC. This has been further verified by a comparison to Waspaloy, which shows an increased susceptibility towards strain age cracking due to its more rapid precipitation kinetics and reduced carbide stability. Apart from microstructural evolution, grain size has been found to be a main factor governing the ductility response.

8. Future work

The effect of Laves phase on the weld cracking behaviour of cast ATI 718Plus® should be investigated in more detail. It is suggested to carry out further temperature profile simulations using the Gleeble system to better understand the active liquation and solidification mechanisms of the alloy. The effect of minor elements such as boron should also be investigated, e.g. by using secondary ion mass spectroscopy (SIMS) analysis.

The repair welding studies provided valuable information on realistic performance of the investigated materials. Nonetheless, the tests only evaluate a single weld geometry, i.e. they do not allow for a variation in weld thermal stresses. As such, the investigation of more geometries or using a more controlled setup, as the Varestraint test does, could provide insight into the materials' weld cracking characteristics over a range of stress levels and test parameters.

The SAC investigations were carried out on base material with different heat treatments to investigate the effect of microstructural changes. Since SAC typically occurs in the HAZ of welds, testing microstructures obtained after a HAZ thermal cycle simulation is a logical next step. It was found that the grain boundary condition is of high importance for the SAC mechanism. Consequently, it is suggested to study the evolution of grain boundary precipitates in more detail by advanced material characterisation. It would furthermore be interesting to study the deformation mechanism on the grain boundaries and if grain boundary strength can be enhanced via special pre-weld heat treatments.

It is further suggested to investigate the SAC susceptibility of other, more recently developed materials such as ATI 718Plus®. Considering the application of different material forms in the manufacturing of aerospace components, investigating the effect that microstructures resulting from different production routes such as casting can have on SAC susceptibility could add further to the understanding of weld cracking in nickel-based superalloys.

Acknowledgements

First and foremost, I would like to thank my supervisor Assoc. Professor Joel Andersson. Thank you for guiding me on my way towards a PhD and to becoming an independent researcher. You have always been available for discussions or when I needed support. I could not have wished for a better supervisor. I would also like to thank my examiner Professor Lars Nyborg and my group leader Professor Uta Klement for their support and for making this research possible.

I spent the main part of my work as a PhD student in the welding group at University West in Trollhättan, where most of the experiments were also carried out. I would like to say thank you to everyone at the Production Technology Centre at University West for making this a great experience.

Many thanks go to my fellow PhD students Arun, Chamara, Esmaeil, Nageswaran, Paria, Tahira, Sneha, Suhas, Sukhdeep and Vahid for their collaboration and discussions. I thank all my colleagues from the department of Industrial and Materials Science at Chalmers for a friendly work environment. I always feel welcome when I am there to teach or to carry out experiments.

I want to thank Kjell Hurtig and Mats Högström from University West for all their support and guidance regarding technical equipment and especially for always finding quick solutions to technical problems. Over the years, I spent quite some time at the electron microscopes. Thank you to Yiming Yao, Chalmers University of Technology, and Kenneth Andersson, University West, for the good training and the help whenever something did not work as expected.

From the department of Mechanical Engineering at the University of Manitoba, Canada, I would like to thank Professor Olanrewaju Ojo for inviting me for a research visit to his department. I am sincerely grateful for all the detailed discussions and the feedback I received. I want to thank Dr. Abdul Khaliq Khan for the countless hours spent at the TEM with me and for the immense help with data acquisition and analysis. Special thanks go to Asala Gbenga for the all the help during my stay and the nice discussions.

I want to thank Eva Bränneby and Victoria Sjöstedt at University West and Jessica Twedmark at Chalmers University of Technology for their administrative support.

I am very grateful for the support I received from GKN Aerospace Sweden AB. I would like to specifically thank Bengt Petterson, Géraldine Puyoo and Ceena Joseph for the discussions and feedback in reference group meetings. Thanks also go to Roland Stridh, Patrik Karlsson, and Jerry Isoaho for carrying out welding operations and Andreas Lindberg for his help with sample machining.

I highly appreciate the financial support I received from the Consortium Materials Technology for Thermal Energy Processes (KME) through funding from the Swedish Energy Agency and GKN Aerospace Sweden AB and the funding from the Swedish Agency for Economic and Regional Growth through the European Union – European Development Fund. I also want to thank the Knowledge foundation for financially supporting my research visit to the University of Manitoba, Canada, via the research school SiCoMap.

I would also like to say thank you to my friends Andreas, Nageswaran, Sukhdeep, Wellington, and Xiaoxiao for all the good times and for making it easy to forget work for a while.

Finally, I want to thank my family for their support and encouragement. I would not be here today without you! Edgar and Victoria, thank you for being there for me with your love and support, and for being understanding of me often working late and being somewhere else with my mind. I love you!

References

1. Decker RF (2006) The evolution of wrought age-hardenable superalloys. JOM 58:32–36. https://doi.org/10.1007/s11837-006-0079-8
2. Sjöberg G (2010) Casting Superalloys For Structural Applications. In: 7th International Symposium on Superalloy 718 and Derivatives. The Minerals, Metals & Materials Society, pp 117–130
3. Schafrik RE, Ward DD, Groh JR (2001) Application of alloy 718 in GE aircraft engines: past, present and next five years. In: Superalloys 718, 625, 706 and Various derivatives. The Minerals, Metals & Materials Society, pp 1–11
4. Lefebvre AH, Ballal DR (2010) Gas Turbine Combustion: Alternative Fuels and Emissions. Taylor & Francis, Boca Raton
5. Donachie MJ, Donachie SJ (2002) Superalloys A Technical Guide. ASM International, Materials Park, OH
6. Stoloff NS (1990) Wrought and P/M Superalloys. In: Metals Handbook. ASM International, Materials Park, OH, pp 950–980
7. DuPont JN, Lippold JC, Kiser SD (2009) Welding metallurgy and weldability of nickel-base alloys. Wiley, Hoboken, N.J.
8. Bürgel R, Maier HJ, Niendorf T (2011) Handbuch Hochtemperatur-Werkstofftechnik Grundlagen, Werkstoffbeanspruchungen, Hochtemperaturlegierungen und -beschichtungen. Springer Fachmedien Wiesbaden, Wiesbaden
9. Sims CT, Stoloff NS, Hagel WC (1987) Superalloys II. Wiley, New York
10. Reed RC (2006) The Superalloys Fundamentals and Applications. Cambridge University Press, Cambridge, UK; New York
11. Andersson J, Sjöberg G, Hänninen H (2011) Metallurgical Response of Electron Beam Welded Allvac 718PlusTM. In: Hot Cracking Phenomena in Welds III. Springer Berlin Heidelberg, pp 415–429
12. Knorovsky GA, Cieslak MJ, Headley TJ, et al (1989) INCONEL 718: A solidification diagram. Metall Trans A 20:2149–2158. https://doi.org/10.1007/BF02650300
13. Cao W-D, Kennedy RL (1997) Effect and Mechanism of Phosphorous and Boron on Creep Deformation of Alloy 718. In: Superalloys 718, 625, 706 and Various Derivatives. pp 511–520
14. Allegheny Technologies Incorporated (ATI) (2013) ATI 718Plus Alloy Product Brochure
15. Haynes International Inc. (2008) Waspaloy alloy product brochure
16. Andersson J (2011) Weldability of precipitation hardening superalloys: Influence of microstructure. Doctoral Thesis, Chalmers University of Technology
17. Andersson J (2018) Review of weldability of precipitation hardening Ni- and Fe-Ni-based superalloys. In: Proceedings of the 2018 Superalloy 718 & Derivatives: Energy, Aerospace, and Industrial Applications. The Minerals, Metals & Materials Society, Pittsburgh, USA, p submitted manuscript
18. Peacock HB, Lundin CD, Spruiell JE (1972) Comparison and Analysis of Residual Stress Measuring Techniques and the Effect of Post-Weld Heat Treatment on Residual Stresses in Inconel 600, Inconel X-750 and René 41 Weldments. WRC Bull 177:1–24
19. Hanning F (2015) Strain Age Cracking of Nickel Based Superalloys. Master Thesis, Chalmers University of Technology

20. Pumphrey WI, Jennings PH (1948) A Consideration of the Nature of Brittleness at Temperatures Above the Solidus in Castings and Welds in Aluminium Alloys. J Inst Met 75:235–256

21. Pellini WS (1952) Strain Theory of Hot Tearing. Foundry 80:125-133;192-199

22. Borland JC (1960) Generalized Theory of Super-Solidus Cracking in Welds (and Castings). Br Weld J 7:508–512

23. Lippold JC (1983) An Investigation of Heat Affected Zone Cracking in Alloy 800. Weld J 62:1s–11s

24. Ojo OA, Richards NL, Chaturvedi MC (2004) Microstructural study of weld fusion zone of TIG welded IN 738LC nickel-based superalloy. Scr Mater 51:683–688. https://doi.org/10.1016/j.scriptamat.2004.06.013

25. Ojo OA, Richards NL, Chaturvedi MC (2006) Study of the fusion zone and heat-affected zone microstructures in tungsten inert gas-welded INCONEL 738LC superalloy. Metall Mater Trans A 37:421–433

26. DuPont JN, Robino CV, Marder AR (1998) Solidification and Weldability of Nb-Bearing Superalloys. Weld J 77:417s–431s

27. Vishwakarma K (2008) Microstructural Analysis of Weld Cracking in 718 Plus Superalloy. University of Manitoba

28. Lippold JC, Sowards J, Alexandrov J, et al (2008) Weld Solidfication Cracking in Solid Solution Strenghtened Ni-Base Filler Metals. In: Böllinghaus T, Herold H, Cross CE, Lippold JC (eds) Hot Cracking Phenomena in Welds II. Springer Berlin Heidelberg, pp 147–170

29. Andersson J (2005) Allvac 718+, Mikrostruktur vid Värmebehandling och Svetsning. Bachelor Thesis, Bergskolan —The Swedish School of Mining and Metallurgy

30. Kelly TJ (1989) Elemental effects on cast 718 weldability. Weld J 68:44s–51s

31. Chaturvedi MC, Chen W, Saranchuk A (1997) The Effect of B Segregation on Heat-Affected Zone Microfissuring in EB Welded Inconel 718. In: Superalloys 718, 625, 706 and Various Derivatives. The Minerals, Metals & Materials Society, pp 743–751

32. Vishwakarma KR, Chaturvedi MC (2009) Effect of boron and phosphorus on HAZ microfissuring of Allvac 718 Plus superalloy. Mater Sci Technol 25:351–360. https://doi.org/10.1179/174328407X243032

33. Vincent R (1985) Precipitation around welds in the nickel-base superalloy, Inconel 718. Acta Metall 33:1205–1216

34. Thompson RG, Dobbs JR, Mayo DE (1986) The Effect of Heat Treatment on Microfissuring in Alloy 718. Weld J 65:299s–304s

35. Huang X, Chaturvedi MC, Richards NL, Jackman J (1997) The effect of grain boundary segregation of boron in cast alloy 718 on HAZ microfissuring—A SIMS analysis. Acta Mater 45:3095–3107. https://doi.org/10.1016/S1359-6454(97)00017-7

36. Ping DH, Gu YF, Cui CY, Harada H (2007) Grain boundary segregation in a Ni–Fe-based (Alloy 718) superalloy. Mater Sci Eng A 456:99–102. https://doi.org/10.1016/j.msea.2007.01.090

37. Chen W, Chaturvedi MC, Richards NL (2001) Effect of boron segregation at grain boundaries on heat-affected zone cracking in wrought INCONEL 718. Metall Mater Trans A 32:931–939

38. Benhadad S, Richards NL, Chaturvedi MC (2002) The influence of minor elements on the weldability of an INCONEL 718-type superalloy. Metall Mater Trans A 33:2005–2017

39. Alam T, Felfer PJ, Chaturvedi M, et al (2012) Segregation of B, P, and C in the Ni-Based Superalloy, Inconel 718. Metall Mater Trans A 43:2183–2191. https://doi.org/10.1007/s11661-012-1085-9

40. Pepe JJ, Savage WF (1967) Effects of Constitutional Liquation in 18-Ni Maraging Steel Weldments. Weld J 46:411s–422s

41. Owczarski WA, Duvall DS, Sullivan CP (1966) A Model for Heat-Affected Zone Cracking in Nickel-Base Superalloys. Weld J 45:145s–155s

42. Radhakrishnan B, Thompson RG (1993) The effect of weld Heat-Affected zone (HAZ) liquation kinetics on the hot cracking susceptibility of alloy 718. Metall Trans A 24:1409–1422

43. Ojo OA, Richards NL, Chaturvedi MC (2004) Contribution of constitutional liquation of gamma prime precipitate to weld HAZ cracking of cast Inconel 738 superalloy. Scr Mater 50:641–646. https://doi.org/10.1016/j.scriptamat.2003.11.025

44. Ojo OA, Richards NL, Chaturvedi MC (2004) Liquid film migration of constitutionally liquated γ' in weld heat affected zone (HAZ) of Inconel 738LC superalloy. Scr Mater 51:141–146. https://doi.org/10.1016/j.scriptamat.2004.03.040

45. Hanning F, Khan AK, Anderson J, Ojo O (2020) Advanced microstructural characterization of cast ATI 718Plus® – effect of homogenization heat treatments on secondary phases and repair welding behaviour. Weld World. https://doi.org/10.1007/s40194-020-00851-0

46. Baeslack WA, Nelson DE (1986) Morphology of weld heat-affected zone liquation in cast alloy 718. Metallography 19:371–379

47. Bengough GD (1912) A study of the properties of alloys at high temperatures. J Inst Met 7:123–174

48. Rhines FN, Wray PJ (1961) Investigation of the Intermediate Temperature Ductility Minimum of Metals. ASM Trans Q 54:

49. Arkoosh MA, Fiore NF (1972) Elevated temperature ductility minimum in Hastelloy alloy X. Metall Trans 3:2235–2240. https://doi.org/10.1007/BF02643237

50. Ramirez AJ, Lippold JC (2004) High temperature behavior of Ni-base weld metal Part II – Insight into the mechanism for ductility dip cracking. Mater Sci Eng A 380:245–258. https://doi.org/10.1016/j.msea.2004.03.075

51. Ramirez AJ, Lippold JC (2005) New Insight into the Mechanism of Ductility Dip Cracking in Ni-base Weld Metals. In: Böllinghaus T, Herold H (eds) Hot Cracking Phenomena in Welds. Springer, Berlin, Heidelberg, pp 19–41

52. Noecker F, DuPont JN (2009) Metallurgical investigation into ductility dip cracking in Ni-based alloys: Part I. Weld J 88:7s–20s

53. Noecker FF, DuPont JN (2009) Metallurgical investigation into ductility dip cracking in Ni-based alloys: Part II. Weld J 88:62s–77s

54. Yamaguchi S, Kobayashi H, Matsumiya T, Hayami S (1979) Effect of minor elements on hot workability of nickel-base superalloys. Met Technol 6:170–175

55. Collins MG, Lippold JC (2003) An investigation of ductility dip cracking in nickel-based filler materials-Part I. Weld J 82:288s–295s

56. Nishimoto K, Saida K, Okauchi H (2006) Microcracking in multipass weld metal of alloy 690 Part 1 – Microcracking susceptibility in reheated weld metal. Sci Technol Weld Join 11:455–461. https://doi.org/10.1179/174329306X94291

57. Nishimoto K, Saida K, Okauchi H, Ohta K (2006) Microcracking in multipass weld metal of alloy 690 Part 2 – Microcracking mechanism in reheated weld metal. Sci Technol Weld Join 11:462–470. https://doi.org/10.1179/174329306X94309

58. Nishimoto K, Saida K, Okauchi H, Ohta K (2006) Microcracking in multipass weld metal of alloy 690 Part 3 – Prevention of microcracking in reheated weld metal by addition of La to filler metal. Sci Technol Weld Join 11:471–479. https://doi.org/10.1179/174329306X94318

59. Saida K, Nomoto Y, Okauchi H, et al (2012) Influences of phosphorus and sulphur on ductility dip cracking susceptibility in multipass weld metal of alloy 690. Sci Technol Weld Join 17:1–8. https://doi.org/10.1179/1362171810Y.0000000004

60. Chen JQ, Lu H, Cui W, et al (2014) Effect of grain boundary behaviour on ductility dip cracking mechanism. Mater Sci Technol 30:1189–1196. https://doi.org/10.1179/1743284713Y.0000000431

61. Younger RN, Baker RG (1961) Heat-Afected Zone Cracking in Welded Austenitic Steels During Heat Treatment. Br Weld J 8:579–587

62. Bentley KP (1964) Precipitation During Stress Relief of Welds in Cr-Mo-V Steels. Br Weld J 11:507–515

63. Swift RA (1971) The Mechanism of Stress Relief Cracking in 2-1/4cr-1mo Steel. Weld J 50:195s–200s

64. Shin J, McMahon CJ (1984) Mechanisms of stress relief cracking in a ferritic steel. Acta Metall 32:1535–1552. https://doi.org/10.1016/0001-6160(84)90100-7

65. Meitzner CF, Pense AW (1969) Stress-Relief Cracking in Low-Alloy Steel Weldments. Weld J 48:431s–440s

66. Dhooge A, Vinckier A (1987) Reheat cracking—A review of recent studies. Int J Press Vessels Pip 27:239–269. https://doi.org/10.1016/0308-0161(87)90012-3

67. Dhooge A, Vinckier A (1992) Reheat Cracking—A Review of Recent Studies. Weld World 30:44–71

68. Hughes WP, Berry TF (1967) A Study of the Strain-Age Cracking Characteristics in Welded René 41 - Phase I. Weld J 46:361s–370s

69. Wu KC, Herfert RE (1967) Microstructural Studies of René 41 Simulated Weld Heat-Affected Zones. Weld J 46:32s–38s

70. Prager M, Shira CS (1968) Welding of Precipitation-Hardening Nickel-Base Alloys. WRC Bull 128:1–55

71. Duvall DS, Owczarski WA (1969) Studies of Postweld Heat-Treatment Cracking in Nickel-Base Alloys. Weld J 48:10s–22s

72. Dix AW, Savage WF (1971) Factors influencing strain-age cracking in Inconel X-750. Weld J 50:247s–252s

73. McKeown D (1971) Re-Heat Cracking in High Nickel Alloy Heat-Affected Zones. Weld J 50:201s–206s

74. Franklin JE, Savage WF (1974) Stress Relaxation and Strain-Age Cracking in Rene 41 Weldments. Weld J 53:380s–387s

75. Thamburaj R, Goldak JA, Wallace W (1979) The Influence of Chemical Composition in Post-Weld Heat Treatment Cracking in René 41. SAMPE Q 4:6–12

76. Hanning F, Andersson J (2016) A Review of Strain Age Cracking in Nickel Based Superalloys. In: Conference Proceedings of the 7th International Swedish Production Symposium. Lund, SE

77. Schwenk W, Trabold AF (1963) Weldability of René 41. Weld J 42:460s–645s

78. Andersson J (2014) Weldability of Ni-Based Superalloys. In: Proceedings of the 8th International Symposium on Superalloy 718 and Derivatives. The Minerals, Metals & Materials Society, pp 249–262

79. Carlton JB, Prager M (1970) Variables Influencing the Strain-Age Cracking and Mechanical Properties of René 41 and Related Alloys. WRC Bull 150:13–23

80. Prager M, Sines G (1970) A Mechanism for Cracking During Postwelding Heat Treatment of Nickel-Base Alloys. WRC Bull 150:24–32

81. Berry TF, Hughes WP (1969) A Study of the Strain-Age Cracking Characteristics in Welded René 41 - Phase II. Weld J 48:505s–513s

82. Liu WC, Xiao FR, Yao M, et al (1997) Relationship between the lattice constant of ϒ phase and the content of δ phase, γ″ and γ′ phases in inconel 718. Scr Mater 37:59–64. https://doi.org/10.1016/S1359-6462(97)00064-X

83. Tiley J, Srinivasan R, Banerjee R, et al (2009) Application of X-ray and neutron diffraction to determine lattice parameters and precipitate volume fractions in low misfit nickel base superalloys. Mater Sci Technol 25:1369–1374. https://doi.org/10.1179/174328409X399010

84. Whitmore L, Ahmadi MR, Stockinger M, et al (2014) Microstructural investigation of thermally aged nickel-based superalloy 718Plus. Mater Sci Eng A 594:253–259. https://doi.org/10.1016/j.msea.2013.11.037

85. Dirand L, Cormier J, Jacques A, et al (2013) Measurement of the effective γ/γ′ lattice mismatch during high temperature creep of Ni-based single crystal superalloy. Mater Charact 77:32–46. https://doi.org/10.1016/j.matchar.2012.12.003

86. Thompson EG, Nunez S, Prager M (1968) Practical Solutions to Strain-Age Cracking of René 41. Weld J 47:299s–313s

87. Duvall DS, Owczarski WA (1971) Heat Treatments for Improving the Weldability and Formability of Udimet 700. Weld J 50:401s–409s

88. Idowu OA, Ojo OA, Chaturvedi MC (2007) Effect of heat input on heat affected zone cracking in laser welded ATI Allvac 718Plus superalloy. Mater Sci Eng A 454–455:389–397. https://doi.org/10.1016/j.msea.2006.11.054

89. Gordine J (1971) Some Problems in Welding Inconel 718. Weld J 50:480s–484s

90. Richards NL, Nakkalil R, Chaturvedi MC (1994) The influence of electron-beam welding parameters on heat-affected-zone microfissuring in INCOLOY 903. Metall Mater Trans A 25:1733–1745

91. Kannengiesser T, Boellinghaus T (2013) Cold cracking tests—an overview of present technologies and applications. Weld World 57:3–37. https://doi.org/10.1007/s40194-012-0001-7

92. Kannengiesser T, Boellinghaus T (2014) Hot cracking tests—an overview of present technologies and applications. Weld World 58:397–421. https://doi.org/10.1007/s40194-014-0126-y

93. Leprowski WJ, Monroe RE, Rieppel PJ (1960) Studies on Repair Welding Age-Hardenable Nickel-Base Alloys. Weld J 39:392s–400s

94. Kelly TJ, Cremiso WH, Simon WH (1989) An Evaluation of the Effects of Filler Metal Composition on Cast Alloy 718 Simulated Repair Welds. Weld J 68:14s–18s

95. Quian M, Lippold JC (2002) An Investigation of the Repair Weldability of Waspaloy and Alloy 718. EWI

96. Kayacan R, Varol R, Kimilli O (2004) The effects of pre- and post-weld heat treatment variables on the strain-age cracking in welded Rene 41 components. Mater Res Bull 39:2171–2186. https://doi.org/10.1016/j.materresbull.2004.08.003

97. Andersson J, Sjöberg GP (2012) Repair welding of wrought superalloys: Alloy 718, Allvac 718Plus and Waspaloy. Sci Technol Weld Join 17:49–59. https://doi.org/10.1179/1362171811Y.0000000077

98. Rush MT, Colegrove PA, Zhang Z, Broad D (2012) Liquation and post-weld heat treatment cracking in Rene 80 laser repair welds. J Mater Process Technol 212:188–197. https://doi.org/10.1016/j.jmatprotec.2011.09.001

99. Hanning F, Andersson J (2018) Weldability of wrought Haynes® 282® repair welded using manual gas tungsten arc welding. Weld World 62:39–45. https://doi.org/10.1007/s40194-017-0508-z

100. Savage WF, Lundin CD (1965) The varestraint test. Weld J 44:433–442

101. Lundin CD, Qiao CYP, Lee CH (1990) Standardization of Gleeble Hot Ductility Testing: Part I: Historical Review. In: Weldability of materials: proceedings of the Materials Weldability Symposium held in conjunction with Materials Week, Detroit, MI, 8-12 October 1990. ASM International, Detroit, MI, pp 1–8

102. Mandziej ST (2005) Testing for Susceptibility to Hot Cracking on GleebleTM Physical Simulator. In: Böllinghaus T, Herold H (eds) Hot Cracking Phenomena in Welds. Springer, Berlin, pp 347–376

103. Nippes EF, Savage WF, Bastian BJ, et al (1955) An Investigation of the Hot Ductility of High Temperature Alloys. Weld J 34:183s–196s

104. Peterson B, Krishnan V, Brayshaw D, et al (2010) Castability of 718Plus® Alloy for Structural Gas Turbine Engine Components. In: Proceedings of the 7th International Symposium on Superalloy. The Minerals, Metals & Materials Society, pp 131–146

105. Peterson B, Frias D, Brayshaw D, et al (2012) On the Development of Cast ATI 718Plus® Alloy for Structural Gas Turbine Engine Components. In: Superalloys 2014 Conference. TMS

106. Pike LM (2006) HAYNES® 282™ Alloy - A New Wrought Superalloy Designed for Improved Creep Strength and Fabricability. In: Proceedings of ASME Turbo Expo 2006: Power for Land, Sea and Air. ASME, Barcelona, Spain, pp 1031–1039

107. Haynes International Inc. (2008) Haynes 282 Product Brochure

108. Hanning F, Khan AK, Steffenburg-Nordenström J, et al (2019) Investigation of the Effect of Short Exposure in the Temperature Range of 750–950 °C on the Ductility of Haynes® 282® by Advanced Microstructural Characterization. Metals 9:1357. https://doi.org/10.3390/met9121357

109. Andersson J, Sjöberg G, Chaturvedi M (2010) Hot Ductility Study of HAYNES 282 Superalloy. In: Proceedings of the 7th International Symposium on Superalloy 718 and Derivatives. The Minerals, Metals & Materials Society, pp 539–554

110. Salehi R, Samadi A, Savadkoohi MKh (2012) Influence of Etchants on Quantitative/Qualitative Evaluations of the γ′ Precipitates in a Nickel-Base Superalloy. Metallogr Microstruct Anal 1:290–296. https://doi.org/10.1007/s13632-012-0043-7

111. E04 Committee (1995) Practice for Electrolytic Extraction of Phases from Ni and Ni-Fe Base Superalloys Using a Hydrochloric-Methanol Electrolyte. ASTM International, West Consohocken, PA

112. Fahrmann MG, Pike LM (2018) Experimental TTT Diagram of HAYNES 282 Alloy. In: Ott E, Liu X, Andersson J, et al (eds) Proceedings of the 9th International Symposium on Superalloy 718 & Derivatives: Energy, Aerospace, and Industrial Applications. Springer International Publishing, Cham, pp 565–578

113. Joseph C (2018) Microstructure Evolution and Mechanical Properties of Haynes 282. Doctoral Thesis, Chalmers University of Technology

114. Haas S, Andersson J, Fisk M, et al (2018) Correlation of precipitate evolution with Vickers hardness in Haynes® 282® superalloy: In-situ high-energy SAXS/WAXS investigation. Mater Sci Eng A 711:250–258. https://doi.org/10.1016/j.msea.2017.11.035

115. Joseph C, Persson C, Hörnqvist Colliander M (2017) Influence of heat treatment on the microstructure and tensile properties of Ni-base superalloy Haynes 282. Mater Sci Eng A 679:520–530. https://doi.org/10.1016/j.msea.2016.10.048

116. Hanning F, Khan K Abdul Khaliq, Ojo O, Andersson J (2019) Effect of short-term isothermal exposure on the ductility signature of Waspaloy in the temperature range of 750-950°C – a comparison with Haynes® 282®. submitted for journal publication

117. Whelchel RL, Kelekanjeri VSKG, Gerhardt RA, Ilavsky J (2011) Effect of Aging Treatment on the Microstructure and Resistivity of a Nickel-Base Superalloy. Metall Mater Trans A 42:1362–1372. https://doi.org/10.1007/s11661-010-0483-0

118. Fawley RW, Prager M (1970) Evaluating the Resistance of René 41 to Strain-Age Cracking. WRC Bull 150:1–12

119. Metzler DA (2008) A Gleeble®-based method for ranking the strain-age cracking susceptibility of Ni-based superalloys. Weld J 87:249s–256s

120. Norton SJ, Lippold JC (2002) Development of a new Test Technique to predict Postweld Heat Treatment Cracking. EWI

121. Hanning F, Singh G, Andersson J (2020) The effect of grain size on the susceptibility towards strain age cracking of wrought Haynes® 282®. In: Swedish Production Symposium 2020. Jönköping, Sweden. accepted for presentation.